CHALMERS
UNIVERSITY OF TECHNOLOGY

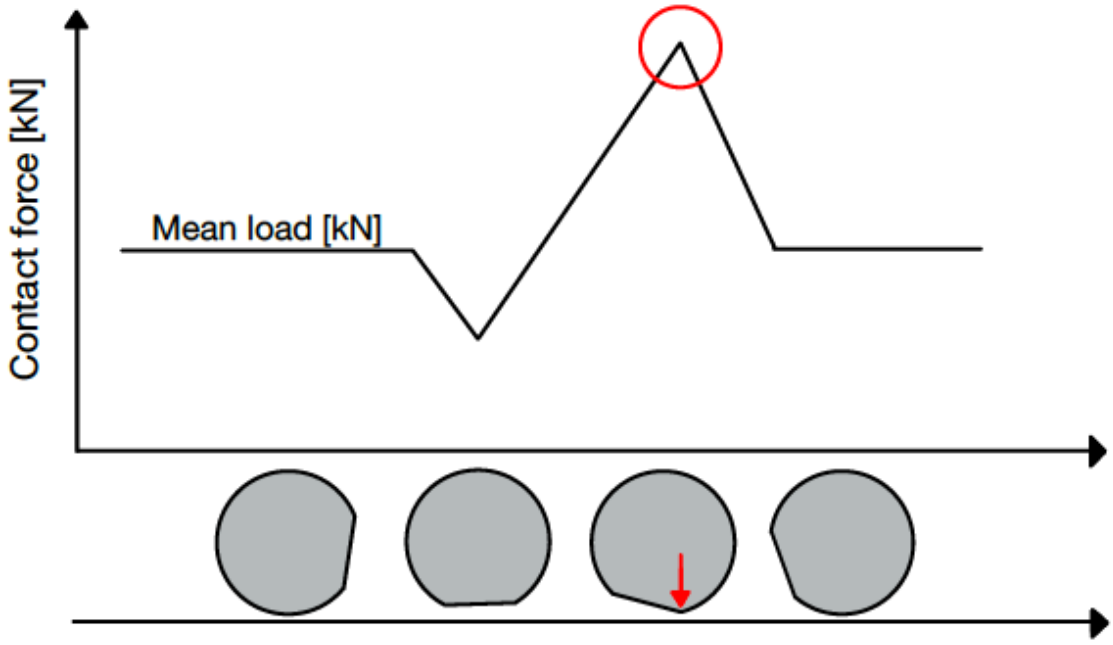

Wheel-rail impact loads generated by wheel flats

Detector measurements and simulations

Master's thesis in Mobility Engineering

KLARA MATTSSON

DEPARTMENT OF MECHANICS AND MARITIME SCIENCES

CHALMERS UNIVERSITY OF TECHNOLOGY
Gothenburg, Sweden 2023
www.chalmers.se

Master's thesis 2023

Wheel-rail impact loads generated by wheel flats

Detector measurements and simulations

KLARA MATTSSON

CHALMERS
UNIVERSITY OF TECHNOLOGY

Department of Mechanics and Maritime Sciences
Division of Dynamics
Centre of Excellence CHARMEC
Chalmers University of Technology
Gothenburg, Sweden 2023

Wheel-rail impact loads generated by wheel flats -
Detector measurements and simulations
KLARA MATTSSON

Supervisors:
Lars Fehrlund, Green Cargo
Andreas Lundin, Green Cargo
Matthias Asplund, Trafikverket
Jens Nielsen, CHARMEC
Michele Maglio, CHARMEC
Tore Vernersson, CHARMEC

Examiner:
Anders Ekberg, CHARMEC

Master's Thesis 2023
Department of Mechanics and Maritime Sciences
Division of Dynamics
Centre of Excellence CHARMEC (CHAlmers Railway MEChanics)
Chalmers University of Technology
SE-412 96 Gothenburg
Telephone +46 31 772 1000

Cover: Principle sketch of time history of vertical wheel-rail contact force induced by a wheel flat. Inspired by similar figures drawn by Matthias Asplund (Trafikverket) and Michele Maglio (Chalmers).

Typeset in LaTeX
Printed by Chalmers Reproservice
Gothenburg, Sweden 2023

Wheel-rail impact loads generated by wheel flats -
Detector measurements and simulations
Master's thesis in Mobility Engineering
KLARA MATTSSON
Department of Mechanics and Maritime Sciences
Division of Dynamics/CHARMEC
Chalmers University of Technology

Abstract

The railway system relies on trains running according to the train schedule to avoid delays, which is why there needs to be as few interruptions as possible. This thesis focuses on wheel tread damage in the form of wheel flats. Based on Trafikverket's regulations, if a flat is longer than 60 mm then the train has to be stopped and the damaged wagon needs to be taken out of service to repair the wheel. The wagons are then put aside on, for example, a passing siding at a station, which could have been used for oncoming trains. This thesis aims to predict wheel-rail impact loads caused by wheel flats, and how variables such as the flat length, axle load, train speed, time since its formation, and unsprung mass influence the load.

The thesis is divided into two main parts: (1) an analysis of measured data from wheel impact load detectors and (2) simulations of vertical dynamic vehicle-track interaction and impact loads. The analysis is performed on wheels that have been removed due to verified wheel flats, by extracting data back in time from when the wheel started to generate a significant increase in peak load. The simulations were carried out on wheel flat geometries that had been 3D-scanned and were performed so that the influence of different axle loads, train speeds, and unsprung masses were considered.

Based on 823 investigated detector passages with wheel flats of different lengths, there was no case of peak load exceeding Trafikverket's high alarm limit 350 kN. This was surprising since several of the investigated cases involved wheel flats longer than 60 mm. No clear correlation between measured impact loads and the variables train speed and flat length was found. This could be due to reasons such as the influence of different lateral offsets between the wheel-rail contact (rolling circle) and the position of the wheel tread damage, and potentially the detector's ability and accuracy to measure high-frequency wheel-rail impact loads.

The simulations were performed for two measured wheel flats, with lengths 75 mm and 120 mm, respectively. For axle load 25 tonnes and train speed 100 km/h, the 75 mm wheel flat with a depth of 1.4 mm reached a maximum peak load of 350 kN. The simulations were performed so that the wheel flat hit the rail at different positions along the sleeper bay. As expected, the most severe case was when the flat hit on top of a sleeper where the track stiffness is higher. The 120 mm wheel flat with a depth of 1.2 mm resulted in significantly lower peak loads, never reaching the high alarm limit of 350 kN. In this case, the maximum calculated peak load was 238 kN

at 25 tonnes axle load and train speed 140 km/h.

A separate analysis to study the accuracy of the detectors to measure static (mean) loads was also carried out. In this study, locomotives on Stålpendeln with known axle loads were used. This indicated a variation in measurement accuracy between the different detectors. It is argued that the calibration of the detectors, as well as variations and differences track stiffness and track geometry at the detector sites might have influenced the results. In addition, for three selected wheel flats, the dynamic loads registered in different detectors along the same southbound or northbound journey (in loaded or unloaded conditions) showed large variations.

The results in this thesis confirm that the depth of a wheel flat has a larger influence on generated impact loads than its length. Further, from both the analysis of wheel impact load detector data and the simulations, the wheel-rail impact loads for a given wheel flat size were found to be lower than expected. Thus, from the findings of this report, it seems more reasonable to base regulations about a wagon's continued operation on measured peak loads than on wheel flat size. Since, for any given wheel flat size, unloaded wagons generally generate lower peak loads than loaded wagons, such regulations would result in more flexibility in allowing unloaded wagons with wheel tread damage to continue their operation to a workshop for repair as long as the alarm limit is not exceeded. If unloaded wagons were allowed to continue (at recommended speed) to their final destination with workshop capabilities, this would lead to fewer traffic disruptions while maintaining safety.

Keywords: Wheel flats, wheel tread damage, wheel-rail impact load, dynamic wheel-rail interaction, wheel impact load detectors.

Stötbelastningar mellan hjul och räl genererade av hjulplattor
Numeriska simuleringar och mätdata från hjulskadedetektorer
Examensarbete inom Mobilitetsteknik
KLARA MATTSSON
Institutionen för Mekanik och Maritima Vetenskaper
Avdelningen för Dynamik/CHARMEC
Chalmers tekniska högskola

Sammanfattning

Järnvägssystemet är beroende av att tågen går enligt tågplaneringen för att undvika förseningar och därför är det viktigt med så få avbrott i trafiken som möjligt. Denna uppsats inriktar sig på en viss typ av skada på tåghjul som kallas hjulplatta, och kan skapa stora förseningar i tågtrafiken i Sverige eftersom vagnar genast måste tas ur trafik om de har en hjulplatta längre än 60 mm. Vagnarna får då placeras på exempelvis på en driftsplats med en extra linje som annars kunde använts till mötande tåg. Denna uppsats syftar till att förstå krafterna som uppstår mellan hjulet och rälsen på grund av hjulplattor och hur olika influerande variabler som längden på plattan, axellasten, hastigheten, tid sedan plattan skapades, samt ofjädrade massan påverkar krafterna.

Arbetet är uppdelat i två huvudområden: (1) analys av data från hjulslagsdetektorer och (2) simuleringar av dynamiska hjul-räl interaktionen och stötbelastningar. Analysen baserades på värden som är samlade från hjulslagsdetektorer och hämtade från hjul som blivit utbytta på grund av hjulplattor. Genom att gå tillbaka i tiden kunde deras utslag i hjulskadedetektorer samlas in. Simuleringarna utfördes på hjul med hjulplattor som var 3D skannade och konstruerades så att det var möjligt att ta axellasten, hastigheten, och ofjädrade massan i beaktning.

Baserat på 823 analyserade detektorpassager med hjulplattor av olika längder, så var det inget fall där maxlasten översteg larmvärdet "hög" på 350 kN. Detta var överraskande eftersom flera av de analyserade fallen involverade plattor med längd över 60 mm. Ingen tydlig koppling kunde hittas mellan mätvärdet från stötbelastningen och variablerna tåghastighet och plattlängd. Detta kan dock bero på anledningar så som den laterala avvikelsen mellan hjul och rälskontakten (rullcirkeln) och positionen av hjulskadan, eller detektorns förmåga att mäta högfrekventa hjul-räl stötbelastningar.

Simuleringarna kördes för två olika hjulplattor, med längderna 75 mm och 120 mm. Vid en axellast på 25 ton och hastighet 100 km/h resulterade hjulplattan som var 75 mm lång och 1.4 mm djup i en maxkraft på 350 kN. Simuleringarna kördes så att hjulplattan träffade olika positioner i sliperspannet. Precis som väntat så inträffade den högsta kraften precis ovanpå en sleeper där rälsstyvheten är högre. Den 120 mm långa hjulplattan med en hjulplatta som var 1.2 mm djup resulterade i betydande lägre krafter, som aldrig översteg alarmvärdet "hög" på 350 kN. I detta fallet, uppstod maxkraften 238 kN vid 25 tons axellast och tåghastigheten 140 km/h.

En separat analys utfördes också för att studera detektorernas mätnoggranhet gällande att mäta statiska (medel) laster. För denna analysen så användes lokomotiv med kända axellaster och analysen visade att detektorernas förmåga att mäta krafter korrekt varierar. I rapporten diskuteras att kalibreringen av detektorerna, precis som spårstyvheten och geometrin på detektorplatsen kan variera och påverkar väldigt sannolikt resultaten. Ytterligare en analys gjordes då tre hjulplattor följdes över tid, och deras registrerade dynamiska laster i detektorer visade stora variationer.

Resultaten från denna rapport styrker att djupet på plattan har en större inverkan än dess längd. Analysen av detektordata och simuleringarna resulterade i lägre hjul-räl krafter än förväntat för en given plattlängd. Baserat på rapportens resultat så verkar det mer rimligt att basera reglerna kring en vagns fortsätta färd på de uppmätta krafterna snarare än plattans längd. Anledningen till det är att oavsett plattlängd så genererar olastade vagnar generellt sätt längre maxlaster än lastade vagnar, och en sådan regel skulle göra det mer flexibelt för en olastad vagn med hjulskada att få köra till en verkstad så länge den inte överskriver larmgränsen. Om olastade vagnar får möjlighet att fortsätta sin färd (med rekommenderad hastighet) till sin slutgiltiga destination med verkstadskompetens kan det leda till färre avbrott i trafiken med fortsatt bibehållen säkerhet.

Nyckelord: Hjulplattor, löpbaneskador på hjul, stötkrafter mellan hjul och räl, dynamisk hjul-räl kontaktkraft, hjulslagsdetektorer.

Acknowledgements

I am very lucky and thankful to have received so much help from my supervisors this spring. I would like to thank Lars Fehrlund and Andreas Lundin, who I initially got in contact with, and from our conversations and your ideas, it was decided that this thesis should focus on wheel flats. Since then, we have had many discussions, and thank you Lars for showing me the world of wheel impact load detectors and always being available for questions and meetings. I also want to thank Matthias Asplund at Trafikverket for being so positive and welcoming about being my supervisor and for a joint project between Green Cargo and Trafikverket.

I have had the opportunity to attend the new master's program in Mobility engineering with the railway profile at Chalmers. During this time I have had the luck to take courses with professors from CHARMEC. My examiner, Anders Ekberg has taught some of them, and thank you for always being available for answering my questions during these two years in the master's program. It is also through the courses at Mobility Engineering I first got in contact with my supervisor Jens Nielsen who has been extremely supportive and helpful this spring. I am very thankful for all your feedback and all the time you have dedicated to helping me every week. I also want to thank Michele Maglio, who besides being invaluable when it comes to helping me perform the simulations, also provided the Green's functions for the track and the wheels. In addition to this, also the models of the wheels with the 3D scanned wheel flats that he had scanned during his work. Thank you also Tore Vernersson who besides helping me with various tasks during the spring also provided the 3D FE models and frequency response functions for the wheelset used in the simulations.

Klara Mattsson, Gothenburg, June 2023

Contents

1

Introduction

Today's railway system is carefully supervised since a healthy condition of track and vehicles is required to avoid harmful damage to components. At the same time, the demands on railway capacity are high and increasing, requiring an efficient maintenance strategy. One of many types of defects that is checked for safety reasons is wheel tread damage on vehicles [1]. A form of wheel damage that is considered to be particulary harmful is the wheel flat as it may generate severe wheel-rail impact loads. These flats occur for several reasons, many of which are related to the wheel sliding on the rail while the train is moving [2]. For example, brake blocks can freeze onto the wheel in the wintertime while a train is waiting for another train to pass [3]. The frozen locked brake can lead to sliding of the wheel, which causes the formation of wheel flats due to wear.

A major issue with wheel flats is that they can damage the rail due to the impact forces generated by the wheel, in some cases even leading to rail breaks. In addition, wheelsets and running gear are also susceptible to damage and failures due to repeated impact loading. This is why the Swedish transport administration requires vehicles with wheel flats longer than 60 mm to stop operating, as the impact load from the wheel in this condition is considered high enough to damage the rail [1]. This regulation can lead to trains having to stop during regular service to disconnect a wagon with wheel flats and to leave it at a station where extra tracks are available. This may cause major problems in traffic since many of the lines in Sweden only have single tracks and those extra lines at stations should be used for oncoming trains. If a train stop is required, it will lead to a high cost due to several reasons. These can for instance be fines to Trafikverket for the delay, increased production costs, and losing money to reimburse customers for their delayed journey. Additional costs are also due to replacing the wheels of the wagon on site, or bringing it to the nearest workshop at reduced speed if permission is given [4].

Wheel flats can be detected by acoustic or visual inspections, and by wheel impact load detectors (WILDs). These are positioned along the track to measure the applied force on the rail, thus making it possible to detect irregularities on the wheels [5]. The detectors will send an alarm if the generated contact force is too high and the train operator will then be informed. In Sweden, there are 30 WILDs spread across the country, with a higher representation in northern Sweden [6]. The train operators are always responsible for making sure the vehicles are safe to operate, independently if they have received a warning alarm from a detector or not [1].

1.1 Research scope

If a detected wheel flat is longer than 60 mm, the vehicle must be detached and taken out of traffic [1]. This regulation holds regardless of parameters such as the axle load of the vehicle, even though a given wheel flat size on an unloaded vehicle will generally lead to lower peak loads. This regulation is a background to the project and one of the reasons why this project was initiated. The main research scope of this project is therefore to investigate correlations between the impact forces generated by a given wheel flat and each of the variables: axle load, train speed, unsprung mass, time since generation of the flat, and flat length to understand more about the magnitudes of impact loads generated by wheel flats. The investigation is based on both analysis of detector data and numerical simulations using a model of vertical dynamic vehicle-track interaction.

2

Literature review

2.1 Wheel flats

A train moving forward while a brake is locked will lead to sliding of that wheel instead of rolling, resulting in extensive wear and the creation of a wheel flat. The varying reasons why the brake may be locked can often be season-related, with a higher frequency of flats occurring in the winter. This relates to what was previously mentioned, a brake block freezing onto the wheel while the train is standing still, for example when waiting for another train to pass. Also, ice on the rail can decrease the adhesion level in the wheel-rail contact and therefore lead to wheel sliding. The adhesion level can also be affected by grease or leaves on the rail which create lower friction [7, 8]. Another reason for a locked wheel can be too-high braking force relative to the available wheel-rail friction as well as the brake not being released after braking. Additional faults related to the braking can be the locomotive driver not being gentle enough when using the brakes or other technical faults related to the braking system [9]. Using wheel slip protection in the braking system can lead to the generation of several small flats but prevents bigger flats to form [10].

Even though current regulations regarding the allowable size of a wheel flat are based on wheel flat length, the more crucial characteristics affecting the magnitudes of impact loads generated by the wheel flat are its shape and depth. Measuring the depth of the flat is not as easy as measuring the length as it both can be problematic and difficult especially while the wheel is on the railway line. The shape of the flat is important as a newly formed flat has sharp edges, which after a while will be worn off to become rounder. This means that a "fresh" wheel flat will lead to higher impact loads than an "old" wheel flat. The depth of the wheel flat is highly related to the generated peak impact force, as well as the occurrence of any momentary loss of contact [11]. It can be seen in figure 2.1 that the contact force first decreases due to the depth of the flat, to later increase when the flat hits the rail. This is related to the vertical movement of the wheel, called the wheel trajectory, which is useful when predicting the wheel-rail interaction [12]. In [13], it is recommended to modify the wheel flat regulations which presently only account for the length to also consider the shape or depth of the flat.

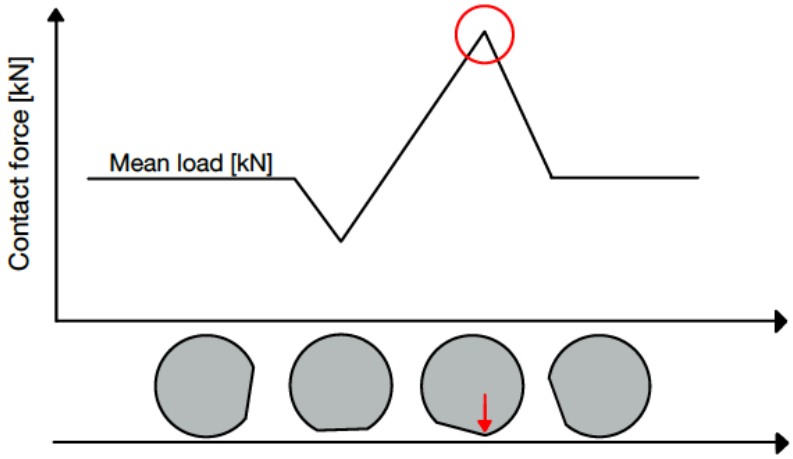

Figure 2.1: Principle sketch of time history of vertical wheel-rail contact force induced by a wheel flat. Inspired by similar figures drawn by Matthias Asplund (Trafikverket) and Michele Maglio (Chalmers)

During the formation of wheel flats, extensive wear occurs, resulting in fast heating of the material which cools down rapidly when the wheel starts to rotate again. A consequence of the rapid cooling of the steel on the wheel surface, can be the formation of martensite. This layer of martensite is brittle and likely to form cracks [14]. These cracks may lead to the fallout of the brittle martensitic steel during the following wheel rotations. The area affected by missing material is denoted as "wheel flat". The formation of wheel flats under controlled conditions was investigated in a field test, see [14]. This study showed that a wheel flat of 40 mm was created due to a locking of the brake for 5 seconds, with an axle load of 10.1 tonnes. However, after locking the brake for 25 seconds, the wheel flat was extended to 50 mm, showing that the formation of wheel flats occurs rapidly at the beginning of a locked brake and then the process slows down.

As previously mentioned, a vehicle with a wheel flat longer than 60 mm should be taken out of operation. The same regulation is also valid if there exists built-up material on the wheel with a height of more than 1 mm. If the wheel flat length is in the range of 40-60 mm, the vehicle can continue without restrictions to its final destination where it should be approved by certified staff before new cargo can be loaded [1]. Related to this is also the general contract of use for wagons (GCU), which is a contract between wagons keepers and railway undertakings used across 20 countries and for around 600 000 wagons in total [15]. This contract also includes regulations about the flat length and for a wheel diameter exceeding 0.84 m, which is normally the case for cargo wagons [9], a wagon should be detached from the train if the flat length is longer than 60 mm. For smaller diameters, the length criterion is stricter [16]. The criterion does not include any information about axle load, meaning that this regulation holds regardless if the wagon is loaded or unloaded.

2.2 Wheel impact load detectors

Wheel impact load detectors are positioned along the track to measure the vertical contact force between rail and wheel. The detectors measure, among other parameters, the mean load and the peak load and these numbers can be used to also provide values of the dynamic load and the ratio. The dynamic load is the difference between the mean load and the peak load, while the ratio is the peak load divided by the mean load. These values are all relevant for different kinds of loaded wagons. The peak load is useful for heavy haul operations to control that the wheels do not apply a load high enough to damage the rail. The dynamic load is useful for wagons that are partially loaded while the ratio is of interest for wagons that are unloaded [10]. Trafikverket has regulations if the loads from the detectors are too high. These are separated into "high" or "warning" alerts. The maximum allowed peak load is 350 kN for a wagon, which if exceeded generates a "high" alarm. In this case, the vehicle can continue at most to the nearest place with extra track available, but only at reduced speed [1]. The alarm limit "warning" means that the vehicle can continue without regulations to its final destination, but from there, it is not allowed to continue operating until it has been approved by certified staff. The numbers for the various limits are presented in table 2.1:

Table 2.1: Alarm limits for wagons set by Trafikverket [17]

Alarm Limit: High	Peak Load	350 kN
Alarm Limit: Warning	Peak Load	280 kN
	Dynamic Load	180 kN
	Ratio	4.8

The limits for locomotives are slightly different, where the alarm limit "high" is instead reached at 425 kN. For the locomotive, there is also a "low" warning alarm at 350 kN. If this limit is reached, the vehicle can continue to operate at reduced speed to at most its final destination with workshop capabilities, where certified staff should inspect the wagon. If the temperature is below -10 C°, train speeds between 15-45 km/h should be avoided [17].

The wheel impact load detectors in operation on the Swedish railway network are of two different types: "SCHENCK" and "PHOENIX MDS WILD" [6]. These have different ways of measuring the contact forces. "SCHENCK" consists of eight consecutive special sleepers where strain gauges are placed between the sleeper and the rail pads to measure the vertical contact force. The shear force is also registered by eight so-called "measuring eyes" that are positioned in drilled holes in the rail [3]. When the rail is loaded, the resulting deformations generate an electrical voltage charge proportional to the applied load [18]. The information that is collected makes it possible to obtain average and peak values of the contact force for each wheel passage. The "PHOENIX MDS WILD" detector on the other hand, uses fibre optic technology mounted on the rail foot to measure the contact force [19]. This is located in the sleeper bay, where the rail will either flex up or down while a train is passing by. The technology then uses fibre optic sensing technology to

provide average and peak values of the impact load. The PHOENIX detector is self-calibrated and covers a measuring span of around 3 revolutions of the wheel. This can be compared to SCHENCK which has a shorter span of measurement [20, 21]. Another difference is that the PHOENIX detector has a higher sampling frequency compared to the SCHENCK detector.

The measured load values from the detectors can include uncertainties due to different reasons. First of all, the calibration of the detectors will include uncertainties. To keep the detectors in a healthy condition, annual maintenance is carried out [22]. The maintenance procedure is different for the two types of detectors but includes tasks such as controlling the hardware and measuring signals. Further, when analyzing the load from a wheel flat, it is not known what lateral position of the wheel that was in contact with the rail. If the centre of the wheel flat hits the rail, its full length (and depth) will influence the generated impact load. On the other hand, if there is a large lateral offset between the center of the flat and the impact position, then a shorter length (and smaller depth) of the flat will be in contact with the rail. This means that a large part of the contact patch might, or might not, be affected by the wheel flat. For a given wheel flat, this will provide uncertainties since it can not be known what lateral position of the wheel that hits the detector. Another circumstance that will affect the contact force and therefore provide uncertainties in the analysis of detector data for data analysis is where within the sleeper bay the wheel flat hits the rail. In [23], it is stated that the track is most stiff above the sleeper which contributes to the generation of a larger impact load. Further, the measured peak load will be influenced by the axle load which can be unevenly distributed between the axles. Therefore, to correlate a certain axle load to an impact load the cargo needs to be evenly distributed between the axles.

To get an understanding of how the magnitudes of impact loads can be distributed, figure 2.2 from [23] is presented below. The data was collected over 6 months from 1 October 2017 to 1 April 2018 from the right rail at "Sunderbyns" impact load detector, located in northern Sweden. The statistics are based on data from freight traffic and the study showed that the alarm limit "high" (peak loads over 350 kN) was exceeded five times, with 455 kN being the highest peak load detected. This can be compared with another period, Feb 2019–Feb 2020, presented in [24] where 30 "high" alarms were detected at Bodsjön. The wheel impact load detector at Bodsjön had the highest amount of "high" alarms in the Swedish railway network during this time span.

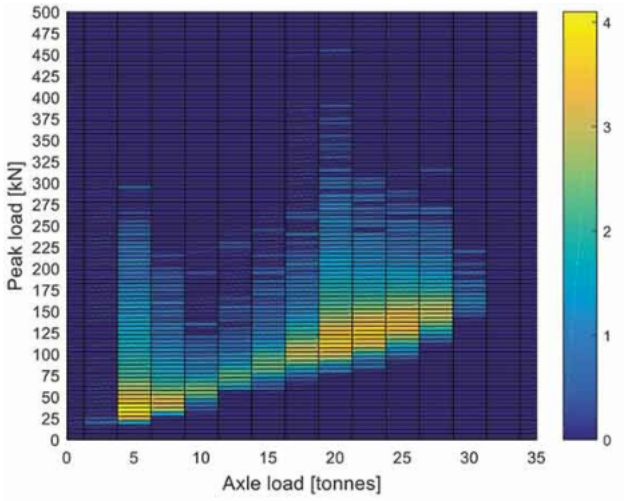

Figure 2.2: Numbers of occurrences of peak load magnitudes (in logarithmic scale, 3 meaning 10^3=1000) versus different levels of axle load. The range of each axle load bin is 2.5 tonnes, while the range of each dynamic load bin is 5 kN. From [23]

2.3 Wheel-rail impact

As previously mentioned, wheel flats can cause damage to track and vehicle components resulting in regulations on their allowed length. The wheel flat length will affect the magnitude of the impact load, shown in figure 2.3 where a simulation [25] demonstrates that a greater length of flat results in a higher wheel-rail contact force. Note that for a given wheel diameter, the length and depth of a new wheel flat are related by the chord theorem.

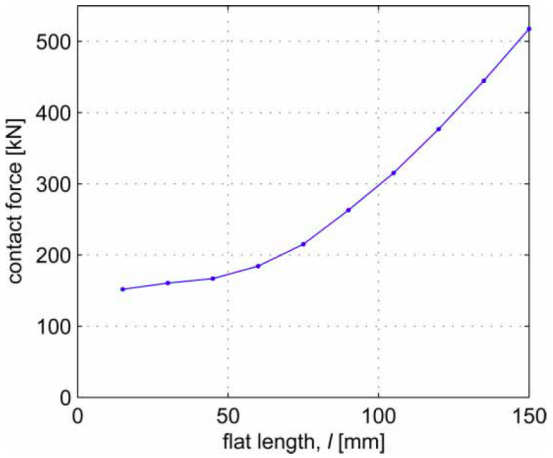

Figure 2.3: Simulation of maximum contact force (peak load) under the conditions studied in [25]. The axle load is 30 tonnes and the speed is 60 km/h. The force 350 kN is obtained around a flat length of 113 mm. According to the formula given in the article, this should correspond to a depth of 1.6 mm of the flat

Other parameters influencing the impact load other than the size and geometry of

the wheel flat are described in [23]. These are the speed of the train, axle load, and the coupled vehicle-track dynamics. In particular, parameters that will significantly influence the vertical load are the unsprung mass and track stiffness. The track stiffness is dependent on the stiffnesses of ballast, subgrade, and rail pads. It is crucial where in the sleeper bay the wheel flat hits the rail, and as previously mentioned one of the worst scenarios is on top of a sleeper due to the higher track stiffness [23]. The increased wheel-rail impact loads due to wheel flats will also cause damage and wear to the components in the vehicles, which is another reason to avoid operating wagons with wheel flats. The influence of the train speed on the forces applied to the rail is studied in [26]. A field test showed that a damaged wheel with the largest depth of 1.8 mm and also an un-roundness in the form of an ovality with radial peak-to-trough offset of 2 mm, resulted in a linear increase in force for speeds between 10-100 km/h.

Field tests have been carried out to investigate the wheel-rail impact force generated by defective wheels. In two different field tests, on Svealandsbanan (2000) and Sannahed (1997), a 100 mm long wheel flat was studied by measuring the contact force. These tests are described in [13], where the axle loads used at Svealandsbanan were 9 and 21 tonnes, and 24 tonnes in Sannahed. In terms of variation of magnitude with respect to train speed, a local contact force maximum could be observed in both tests around at 40 km/h, see figure 2.4. However, none of them gave rise to impact loads exceeding the warning alarm limit of 280 kN set by Trafikverket. The article states that higher contact forces can be reached during other circumstances. An example of this is the Iron Ore line, where wagons operate with axle loads of 30 tonnes. Another example are varying seasonal temperatures, where colder conditions lead to higher stiffness of the track and therefore higher impact loads [13]. Due to the considerable difference in tensile stress in the rail depending on the seasonal temperatures and the resulting effect on crack growth, it is stated that having different limits for allowed wheel defects depending on temperature is well founded in [25].

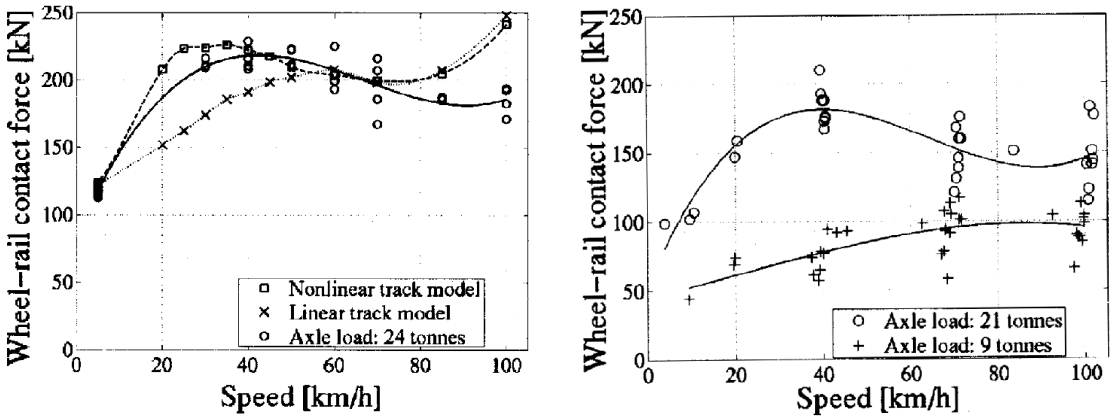

(a) Svealandsbanan 2000.
Flat length 100mm, depth 0.9mm

(b) Sannahed 1997.
Flat length 100mm, depth not stated

Figure 2.4: Measured maximum wheel-rail contact force (peak load) depending on train speed in two different field tests [13]

3

Analysis of wheel impact load detector data

To better understand how the length of the wheel flat, axle load, train speed, and time since the generation of the flat influence the wheel-rail impact load, an extensive analysis of data from wheel impact load detectors was carried out. An additional analysis of the detectors was made to investigate their accuracy in terms of measuring quasi-static (mean) load. The result is presented in various forms of plots.

3.1 Introduction

The analysis has been carried out by extracting data from wheel impact load detectors that are positioned along "Stålpendeln" which is used to haul steel for SSAB, and where the maximum allowed axle load is 25 tonnes [27]. Data from the detectors have been collected from December 2022 to March 2023. In figure 3.1, the locations for the detectors located on Stålpendeln are presented in red and pink. There are a total of nine detectors located on Stålpendeln, where three of them are of the type "PHOENIX MDS WILD", and the rest are of the type "SCHENCK" [6]. However, two of the detectors, located in Mellansjö have been neglected in the analysis, with the motivation that their measuring accuracy is not trusted. Both of these are of the type "PHOENIX MDS WILD". Even though their values are not included in the analysis of the wheel flats, see sections 3.2-3.5, the analysis made on the detectors in section 3.6 includes the two detectors located in Mellansjö.

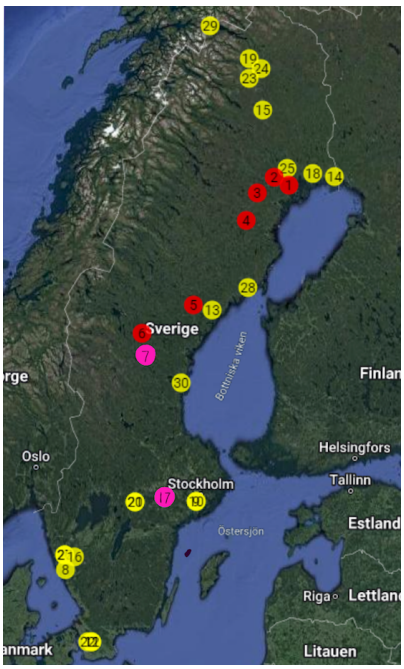

Figure 3.1: Stålpendeln's wheel impact load detectors are marked in pink for "PHOENIX MDS WILD" and red for "SCHENCK" types. Original figure: Green Cargo.

3.1.1 Method for choosing data generated by wheel flats

The analysis started by analysing a document with information about wheel replacements from a workshop in Luleå. This document contained information about when and for what reason a wheel was replaced. If the reason for replacement was a wheel flat, also the length of the wheel flat was specified along with the date of replacement and the date when the wheel damage was discovered. The document was used to create an Excel file that stored information about the wagon number, axle number, flat length, date of discovered damage, and date of replacement for each wheel flat. To understand how the wheel flat affected the forces applied on the rail, information from wheel impact load detectors was compiled for the relevant wagons and period of time. The date of discovered damage that was stated in the document from Luleå was not considered exact enough and might not be the same as when the damage occurred. Therefore, it was used as a starting point to manually find in between which two detectors the wheel flat was created. This could be easily found in the data from the load detectors due to the sudden increase in dynamic forces. If no increase in the dynamic forces was found for an axle between the date of discovered damage and replacement, the data from that axle was not included in the analysis. The reason for this is that the wheel flat could then have been created after passing the detectors, and the analysis should only consist of data from verified wheel flats. In total, there are 823 axle passages from 149 different wheel axles, with at least one of the wheels on the axle being defective, included in the analysis. Figure 3.2 illustrates an example of how four data points were selected.

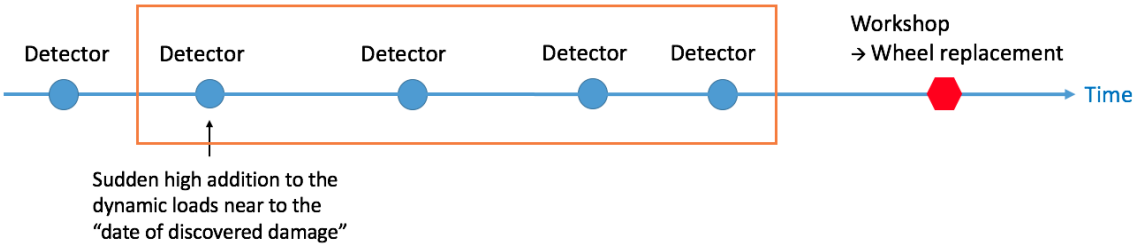

Figure 3.2: A timeline describing the method used to select what impact load detector data that should be included in the analysis. In this example, the data from four passages in the detectors of the same axle would be included in the analysis.

In addition, all data from passages at train speeds below 40 km/h were filtered out since the RFID tag which registers the vehicle is not always accurate for those speeds [4]. A MATLAB [28] script was then written to retrieve the information in table 3.1 from every wheel flat passage in the detectors, meaning that each wheel flat could generate several values if it had passed several detectors before it was replaced, just as in the figure above.

Table 3.1: For each wheel flat passage in a detector, the following information from both wheels on the axle was collected from the detector data.

Mean Load
Dynamic Load
Peak Load
Train Speed
Date and Time
Detector Location

Even though a wheel flat is likely to occur on both wheels on the axle, there can also be cases where only one wheel has a wheel flat or where they have different lengths. Therefore, only the highest peak wheel load on the axle was used in the analysis. This was in order to make sure that the analysis only accounted for wheel flats. Since the peak load for only one wheel was used, the axle load was calculated as the mean load for that defective wheel multiplied by two.

3.1.1.1 Interview with staff measuring the wheel flats

An interview was held with a freight wagon repair worker at Euromaint in Luleå to better understand how the flats were documented and with what accuracy they are measured [29]. The worker explained that they have internal training to learn how to measure a wheel flat. Flats with rounded edges are more challenging to measure and for those cases, only the non-rounded part of the wheel flat is measured. The flat length is stated in millimetre, and a majority of the lengths in the document end with 0 or 5. This could be explained by the challenge of measuring a rounded flat to an exact millimetre. The fact that only the non-rounded part of the wheel flat is measured means that the registered length of a rounded flat is "shorter" when it is measured compared to what it was when it was created. This is because the edges are worn off and therefore the flat part will become shorter, this is confirmed in [2]. Flats that have sharper edges are easier to measure and for those, the measuring accuracy can be better. If there are two types of damage on the same wheel, for example, a wheel flat and rolling contact fatigue cluster, then the wheel flat is always stated in the document. This means that for some wheel flats in the data, there could potentially also be other types of damage influencing the impact loads. The wheel-rail impact loads from the data could then be considered conservative for some cases since a combination of damages contributes to higher loads. If there are several flats on the wheel, which is not very common according to the repair worker, the biggest flat is always documented. The most common case is that both wheels on the axle have a flat on the same angular position, however, they are not always equal in size, and therefore the longest flat is stated in the document.

3.1.2 Unloaded and loaded wagons

The wagons in the analysis are either loaded with steel or unloaded, which means that there is a range of axle loads in the detector data. To find out at what speed the train is running when it is loaded or unloaded, a plot was made with all the

detector passages that were used in the analysis. Figure 3.3 illustrates the results where the axle load is plotted on the x-axis and the speed on the y-axis. The ranges in terms of train speed and axle load that are relevant for the analysis were then chosen. Based on the result, it was determined that the analysis would be focused on "Unloaded" and "Loaded" wagon cases. These values were chosen so that as much data as possible would be included, but data points that did not have relevant speed or axle load were removed.

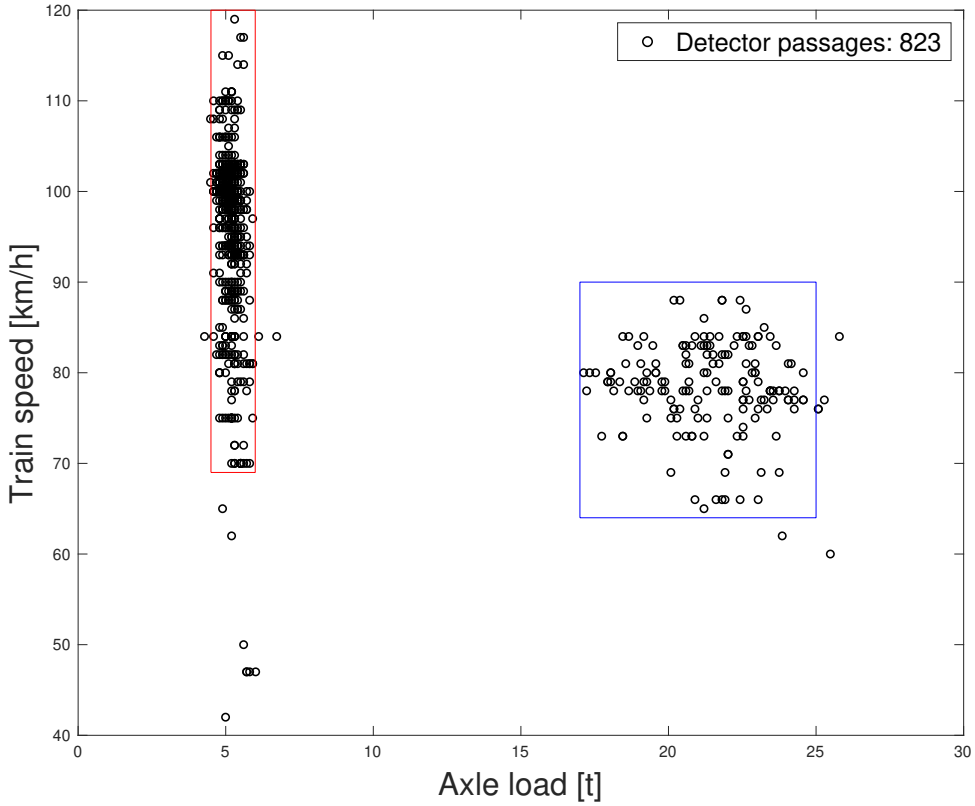

Figure 3.3: All collected data collected from wheel impact load detectors. The red and blue boxes respectively indicate which range of values were used as the "Unloaded" and "Loaded" cases in the analysis. Note that some data points overlap each other.

The analysis of unloaded wagons consisted of wagons with axle loads between 4.5–6 tonnes and speeds between 69–120 km/h. The amount of passages over the detectors for the unloaded case was 645. The loaded wagons, on the other hand, have a range of axle loads between 17–26 tonnes and speeds between 64–90 km/h. The number of passages for the loaded cases was 159.

The reason why there is more data for the unloaded case could be that the train leaves Luleå with loaded wagons to travel southwards. When the wagons reach their destination, the cargo is unloaded and the wagons travel back north to Luleå where the workshop is located. If the wheels are damaged and have been setting off warning alarms, they are checked by certified staff in Luleå and are likely to be replaced. This means that even if the damage on the wheel occurs on the way south

in the loaded case, the wagons return in the unloaded case through the detectors. This presupposes that the warning limit "high" was not reached or that a wheel flat bigger than 60 mm was not discovered because in this case, the wagon would not be allowed to continue its regular service.

3.2 Wheel flat load data in relation to alarm limits

A plot was made with all data to understand how many of the wheels in the data set would generate an alarm, both in the unloaded and loaded cases. Table 2.1, in chapter 2, presented Trafikverkets alarm limits. In figure 3.4 the highest peak load generated by one of the wheels on each axle passing a detector is shown. The axle load was calculated as the defective wheel's mean load multiplied by two. In the figure, it can be seen that most warning alarms have been set off for unloaded wagons in the form of ratio alarms with axle loads of around 5 tonnes. However, there are around four times as much data from the unloaded case compared to the loaded case which can contribute to some extent that more alarms come from the unloaded case. What can also be noticed in the figure is that there is no data from any size of wheel flat or axle load that exceeded the high alarm limit at 350 kN.

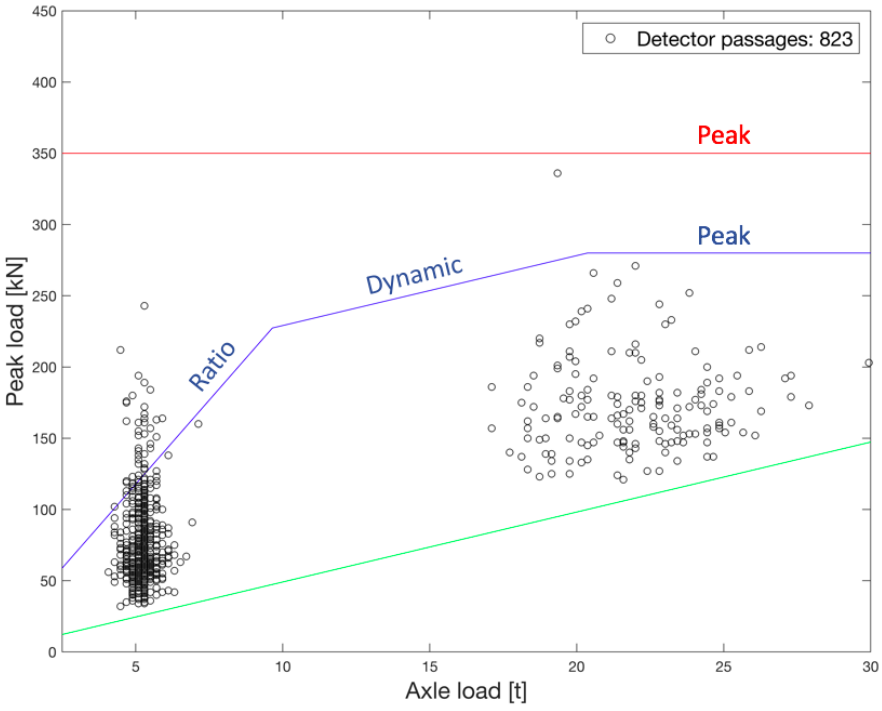

Figure 3.4: The green line represents the axle load in tonnes on the x-axis and the corresponding mean load from one wheel in kN on the y-axis. Thus, if there were no dynamic loads, all the data points would be located on the green line. The blue line indicates warning levels in terms of ratio (axle loads up to 10 tonnes), dynamic load (axle loads in the interval 10–20 tonnes), and peak load. The red line illustrates the "high" alarm at 350 kN.

3.3 Influence of flat length and train speed

For different intervals of wheel flat length, figure 3.5 and 3.6 present detected peak loads versus train speed. A linear regression has been made to indicate any possible linear trend of the data, but this could not be confirmed. Due to having more data from unloaded vehicles, more flat lengths could be included in the analysis for the unloaded wagons. In each subplot, one colour represents one specific wheel flat. This means that if the same colour occurs several times in a given subplot, that wheel flat has passed several detectors. Note that for the two wheels on an axle, the highest peak load was always chosen from each detector passage, therefore the same colour could potentially represent either the left or the right wheel on an axle in some cases. Another important aspect to point out is that the same colour in two different subplots does not have any correlation. The linear regressions R-square value is presented in each subplot along with the amount of data points, where a perfect fit between the points and line would give an R-square value of 100%.

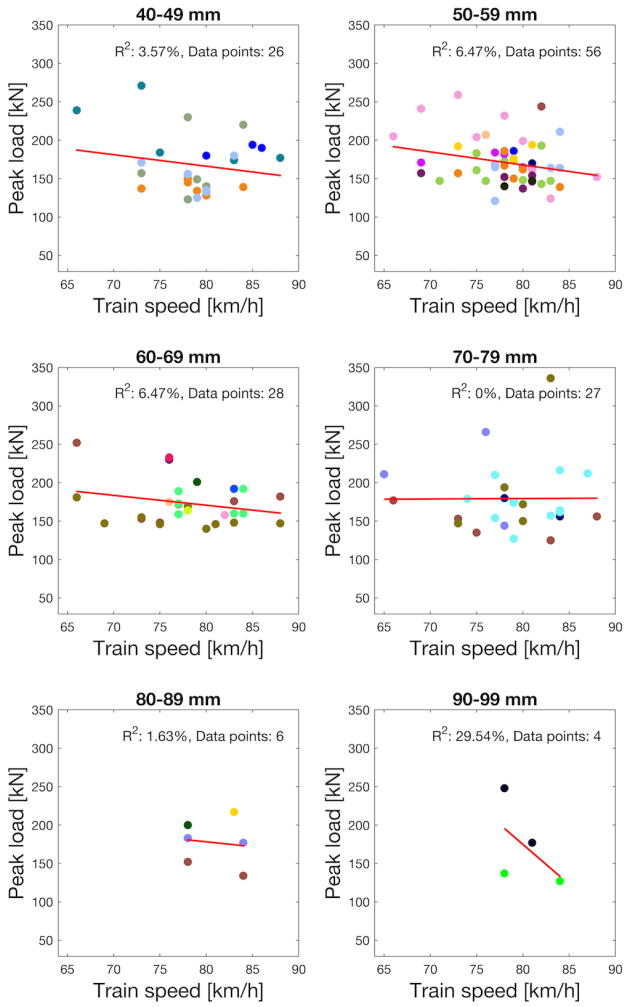

Figure 3.5: Influence of wheel flat length interval on peak loads for loaded wagons weighing between 17–25 tonnes.

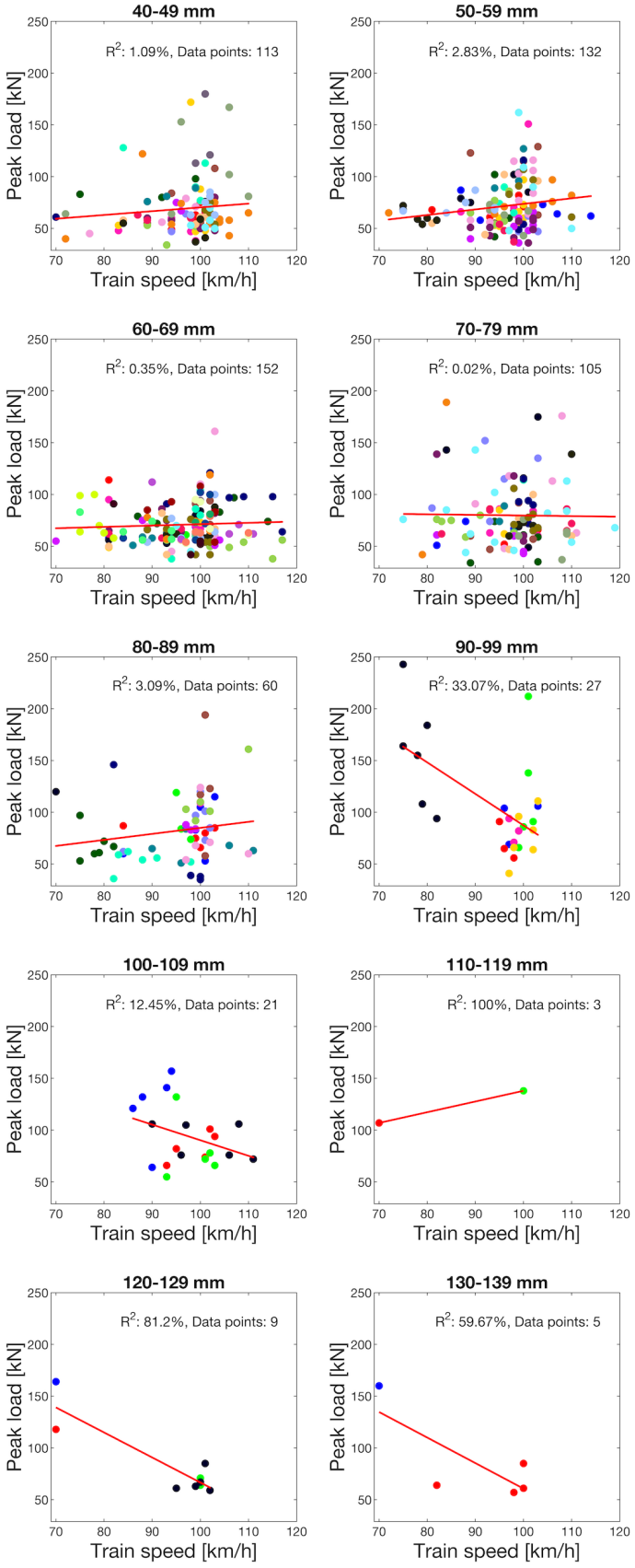

Figure 3.6: Influence of wheel flat length interval on peak loads for unloaded wagons weighing between 4.5–6 tonnes.

As can be seen in the figures, the R-square value is very low in most subplots. This indicates that there seems to be no linear correlation between peak load and train speed in the set of data measured by the detectors. However, the reason for this has been pondered upon and, as previously mentioned, there are several uncertainties regarding measured values from wheel impact load detectors. One reason for the big spread in the data could be that the lateral position of the wheel in contact with the rail over the detector is not the same for the different passages. This means that for one detector, the full flat could have hit the rail while for the next one, the wheel-rail contact might have occurred towards the edge of the flat. Another uncertainty is the measuring accuracy and calibration of the detectors. The calibration is likely to differ between the detectors. Other reasons could be related to the position within the sleeper bay where the flat hits the rail and if the flat has rounded edges or not. From the literature review, it was clear that the depth of the wheel flat has a larger influence than its length, but the depth is not known which also contributes to the uncertainties along with variations in the unsprung mass and the variation in track stiffness between different detectors. Further, no clear expected correlation between wheel flat length and peak load could be detected, which is surprising.

In Appendix A (see figures A.5, A.6) similar plots where impact loads are shown as a function of the flat lengths and the subplots were sorted depending on the vehicle speed are presented. The figures illustrate that the peak loads from the loaded cases are higher, which makes sense since the mean (quasi-static) loads are higher. Similar plots are also presented in the form of dynamic loads and ratios, presented in appendix A (see figures A.1 - A.4). These figures show a slightly higher value in dynamic loads for the loaded case than for the unloaded. As expected the ratio values for the unloaded wagons are higher than for the loaded case.

3.4 Cumulative distribution of peak loads

Figure 3.7 and 3.8 present the cumulative distribution related to the same data as in the plots above. The peak load is represented on the x-axis and the probability that the peak load will reach that value or a value below is presented on the y-axis. The red line indicates the high alarm limit of 350 kN, while the orange dashed line is the warning alarm of 280 kN. The figures show that the high alarm limit was never exceeded for the entire set of data studied in this work. However, it is important to point out that this does not mean that this limit could not be reached for these wagons and flat lengths under other circumstances. The lateral position of the contact patch, depth of the flat, and the location in the sleeper bay where the wheel flat hit the rail are both determining the peak load, and it can not be known if the most severe combination for this occurred in any of the data included in this report. What also is unknown is the detector's capability of measuring peak loads accurately. Nevertheless, based on the relative large data set used in this study, it can be concluded that the probability that a wheel flat with length at least up to 100 mm would generate an impact load exceeding the alarm limit is low.

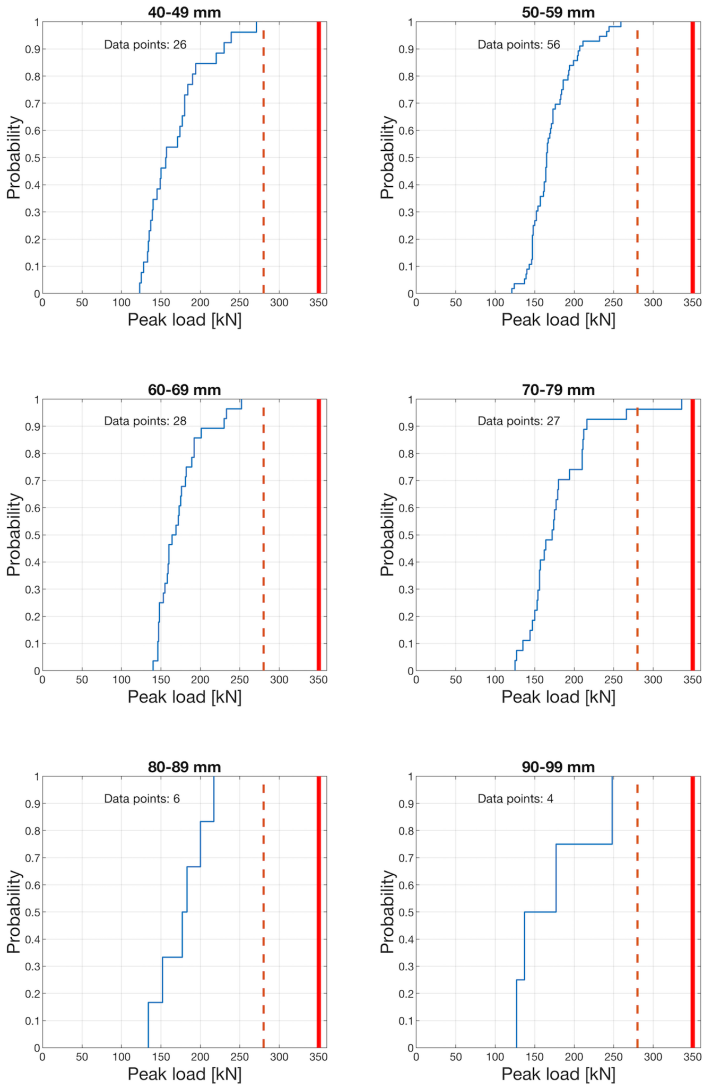

Figure 3.7: The cumulative distribution of peak loads for loaded wagons with axle load between 17–25 tonnes.

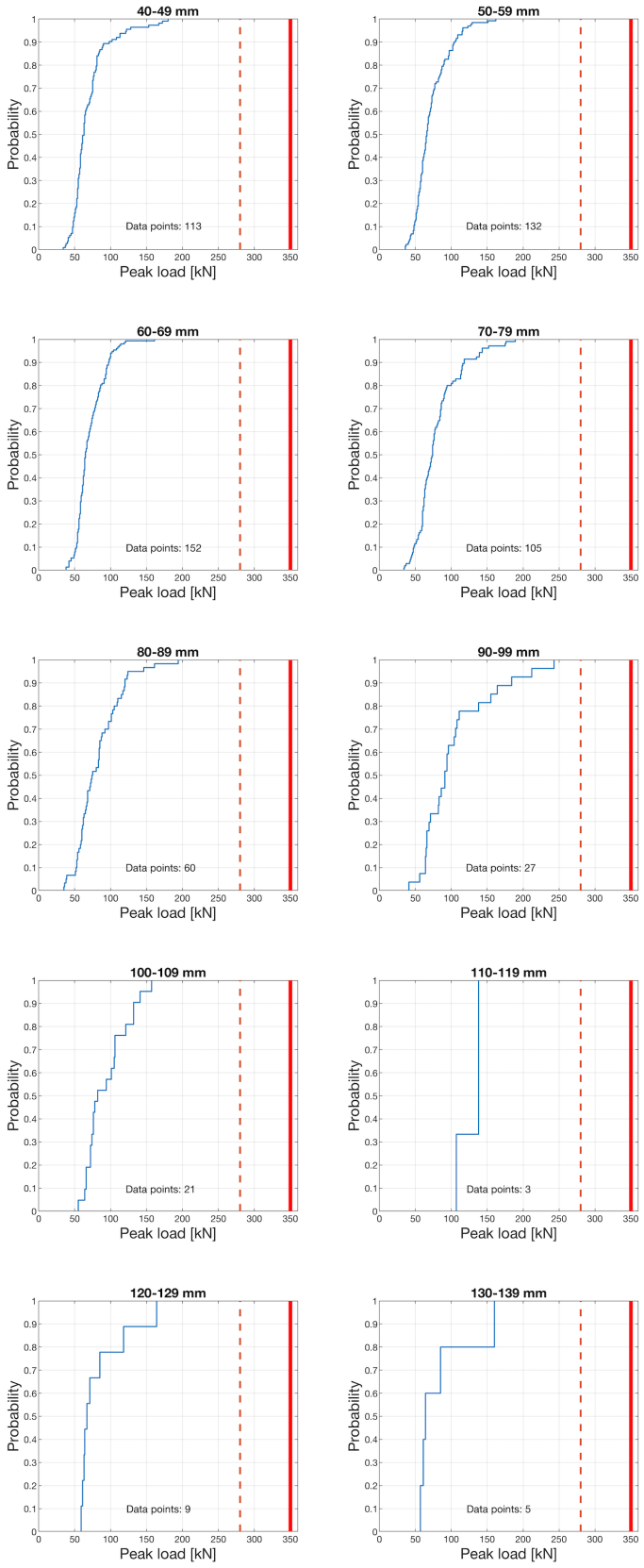

Figure 3.8: The cumulative distribution of peak loads for unloaded wagons with axle loads between 4.5–6 tonnes.

3.5 Detector history for a given wheel flat

An analysis of how the mean and peak load values vary over a period of time for a given wheel flat while passing different detectors was made. The wheel flats chosen to be analyzed were those with the highest numbers of registered data from the date of the generation of the wheel flat to the date of replacement. In this analysis, the wheel in each axle generating the highest peak load was chosen and followed over time. The analysis was also designed to discriminate between the different detectors the data were collected from. For a given wheel flat, the analysis can therefore also be used to see how the measured forces vary between different detectors.

Figures 3.9, 3.10 and 3.11 show how the measured peak load from three different wheel flats changes over time, and the analysis includes values from both unloaded and loaded wagons. On the black left vertical axis, the peak load is presented in kN, while the axle load is presented in tonnes on the red right vertical axis. From the plot (red curve), it is possible to see whether the wagon was unloaded or loaded. The "axle load" is the mean load of the defective wheel multiplied by two.

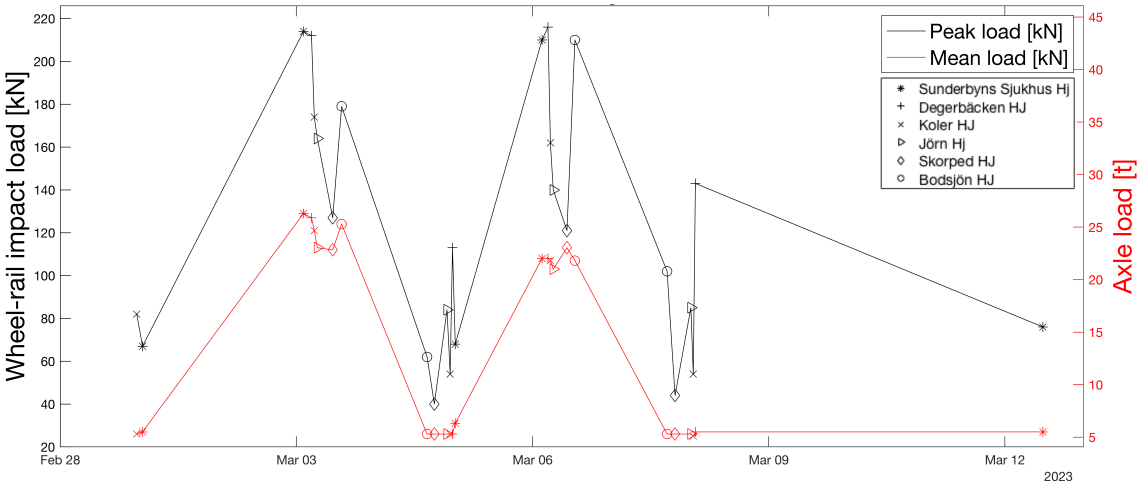

Figure 3.9: Peak loads generated by a wheel flat with length 75mm. The corresponding train speeds based on order according to the date of the measurement in km/h:
Speed for unloaded: 105, 62, 89, 98, 109, 110, 109, 119, 94, 88, 84, 94, 90 km/h
Speed for loaded: 62, 87, 79, 84, 79, 74, 77, 84, 84, 83, 77, 77, 75 km/h

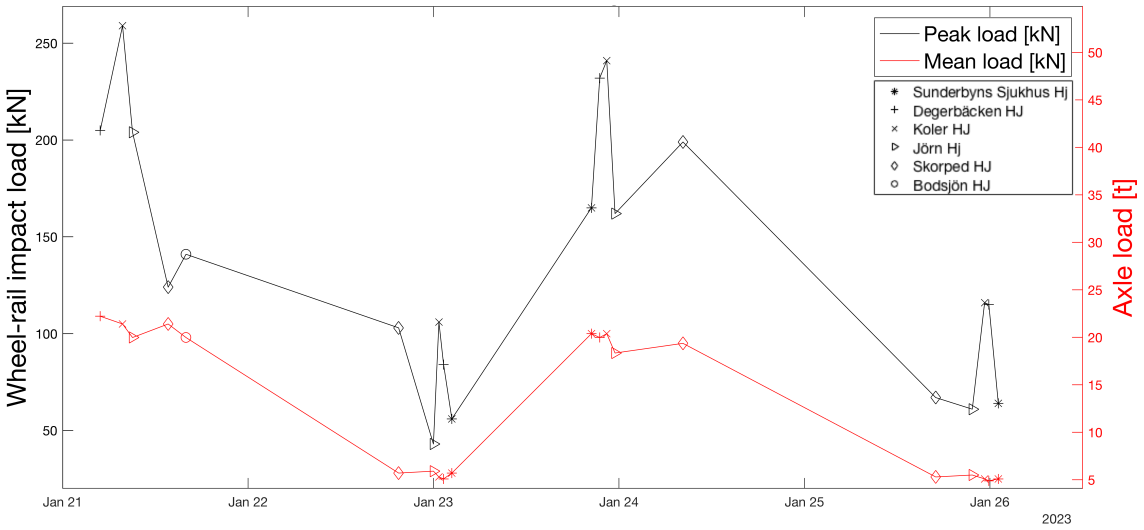

Figure 3.10: Peak loads generated by a wheel flat with length 55 mm. The corresponding train speeds based on order according to the date of the measurement in km/h:
Unloaded: 99, 89, 102, 102, 93, 93, 99, 102, 98, 101 km/h
Loaded: 66, 73, 75, 83, 88, 77, 78, 69, 81, 80 km/h

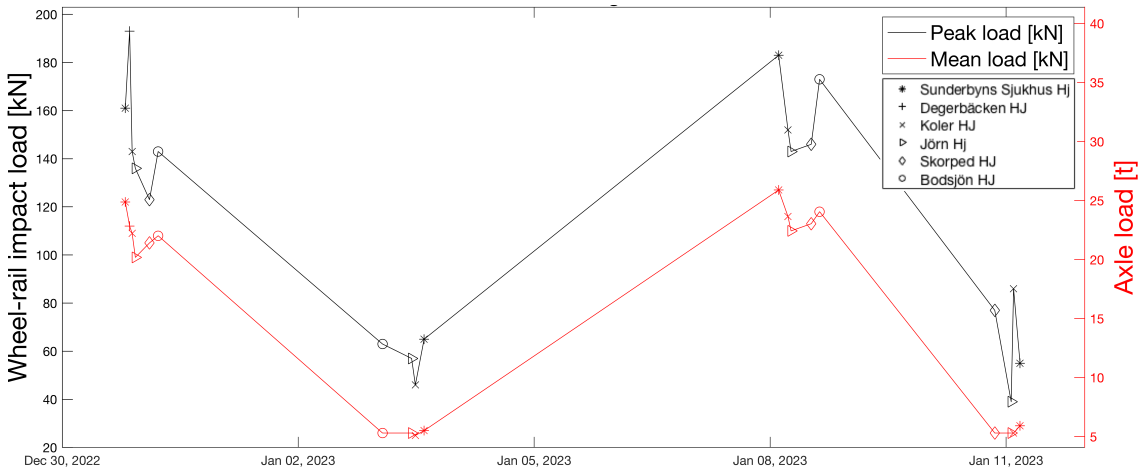

Figure 3.11: Peak loads generated by a wheel flat with length 50mm. The corresponding train speeds based on order according to the date of the measurement in km/h:
Unloaded: 42, 96, 93, 89, 94, 94, 97, 47 km/h
Loaded: 75, 82, 75, 76, 83, 82, 76, 77, 71, 80, 78 km/h

It is not possible to notice an overall decrease trend in peak loads over time, which might have been expected since the edges of the flat should be rounded off after a while. The dynamic load can be distinguished as the difference between the peak and mean loads (black and red lines). In figures 3.9 and 3.10, it can be observed that the dynamic loads for the loaded cases are higher than for the unloaded case, which disagrees with figure 3.11 where the dynamic loads are similar magnitudes for both cases. What also can be noticed is how differently the detectors measure the forces from the same wheel flat, which can help in understanding the big scatter presented in the previous plots. This can of course, as previously mentioned, depend on for example the wheelset lateral position and differences in train speed. However, in figure 3.9 a very clear pattern in how the detectors measure relatively to each other can be noticed. This indicates that besides the lateral positions and other influencing variables, the calibration of the detectors seems to affect the measured values and the analysis.

3.6 Comparison of mean loads measured in different detectors

An analysis of the detectors was carried out by collecting the measured mean loads from the locomotives driving "Stålpendeln". These are Transmontana locomotives (called Mb-locomotives), each consisting of two bogies with three axles each [30]. All the passages over wheel impact load detectors were collected throughout the four months of December 2022 to March 2023. For each wheelset, the mean loads of both wheels on the axle were summed and divided by the average axle load of the locomotive, which was taken as the total weight (125 tonnes) divided by six. The weight of the locomotives can vary due to ice accumulating in their bogies during the winter and is also depending on whether the wheels are new or reprofiled [4]. The analysis was made on the detectors' capability to measure mean loads, which may differ from their accuracy of measuring peak loads.

Figure 3.12 below presents the analysis carried out for the detectors on Stålpendeln. Since the value registered by the detector is divided by the locomotive's mean axle load, a value above one on the y-axis means that the detector registered a higher value than the assumed axle load of the locomotive. A linear regression has been made on all the data in each plot.

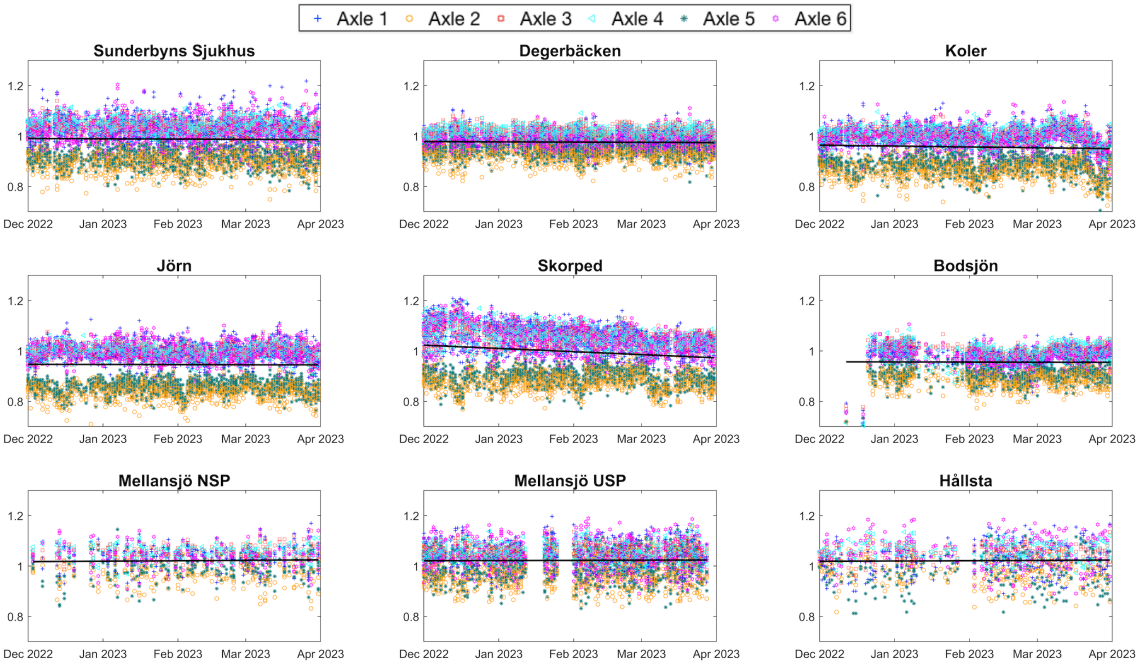

Figure 3.12: Ratio between measured mean load and assumed axle load for the detectors located on Stålpilen. The first and second rows contain detectors of the type "SCHENCK", while the last row contains the three detectors of the type "PHOENIX MDS WILD"

It can be noticed that the detected loads for axles 2 and 5 are consistently lower than those detected for the other axles. Axles 2 and 5 have in common that they are both positioned in the middle of the three-axle bogie. To understand how the weight of the locomotive on the different axles is distributed, an interview was held with a locomotive technician [31]. He described that the locomotive is weighed using a scale built by pieces of rail, and with the help of this, it is possible to adjust the weight between the axles with very good accuracy. The axles should be adjusted at least once a year, or when replacing an axle on the locomotive. Even though the locomotive leaves the workshop with very good weight distribution on the axles, it is common for the locomotive to come back to the workshop with slightly lower axle loads on axles 2 and 5.

What can be noticed from the subplots in figure 3.12, is the space in the middle that separates the measurements from axles 2 and 5 from the other axles. This space varies a lot between the different detectors, and the reason for this has been discussed. It can be due to the calibration of the detectors, however, it might also be influenced by the stiffness of the supporting track foundation.

4

3D laser scanning of wheel damage

To be able to simulate vertical wheel-rail contact forces generated by wheel flats, 3D laser scanning has been carried out on the surface of two damaged wheels. The wheels were scanned on different occasions, in 2018 and 2022, within another project [32]. The laser tool used to scan the surface of the wheel flat is called HandySCAN [33] and is shown in figure 4.1. Only the section of the wheel tread including the wheel flat was scanned and then that surface was superposed to the surface of an undamaged wheel. The wheel flats used in the simulations are presented in sections 4.1 and 4.2.

Figure 4.1: The HandySCAN tool used to scan the surface of the damaged wheel

The 3D scanning in combination with numerical simulation makes it possible to analyze the influence of different lateral contact positions on the wheel. Depending on where the lateral position of the wheel is in contact with the rail, the geometry of the section of the wheel flat interacting with the rail is different. The lateral position is often referred to as the rolling circle, and the simulation takes this position

into consideration. Figure 4.2 illustrates a wheel and demonstrates how the lateral positions, in 5 mm intervals, are labelled in the simulations. Position 5 is the nominal rolling circle that is located 70 mm from the flange side of the wheel rim. The diameter of the wheel is given at the position of the nominal rolling circle [34].

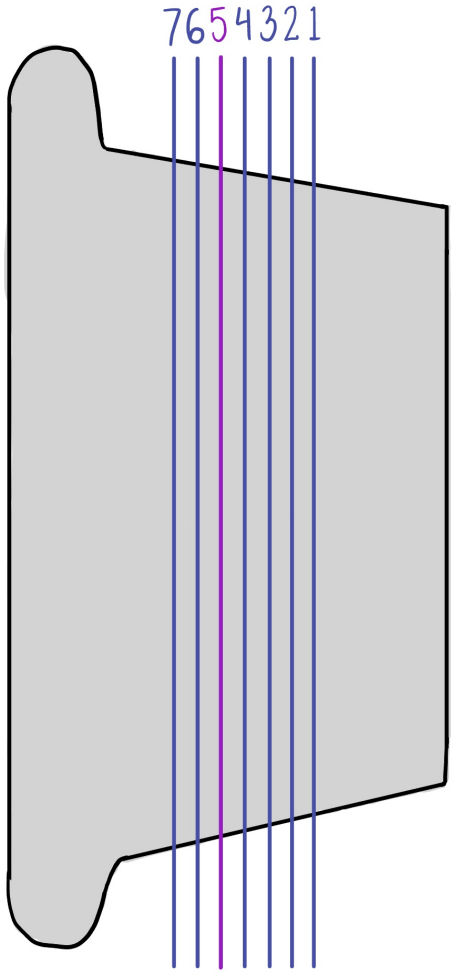

Figure 4.2: The lateral positions used in the simulations

4.1 Wheel flat 1 - 75 mm

The first wheel tread damage is from now on named "Wheel flat 1" and consists of a wheel flat with approximately a length of 75 mm, see figure 4.3a. The other wheel on the axle had a wheel flat with a length of around 50 mm, see figure 4.3b. Figure 4.4, illustrates the wheel flats' radial deviation from the nominal wheel surface at different lateral positions. The deepest part of the flat is 1.4 mm.

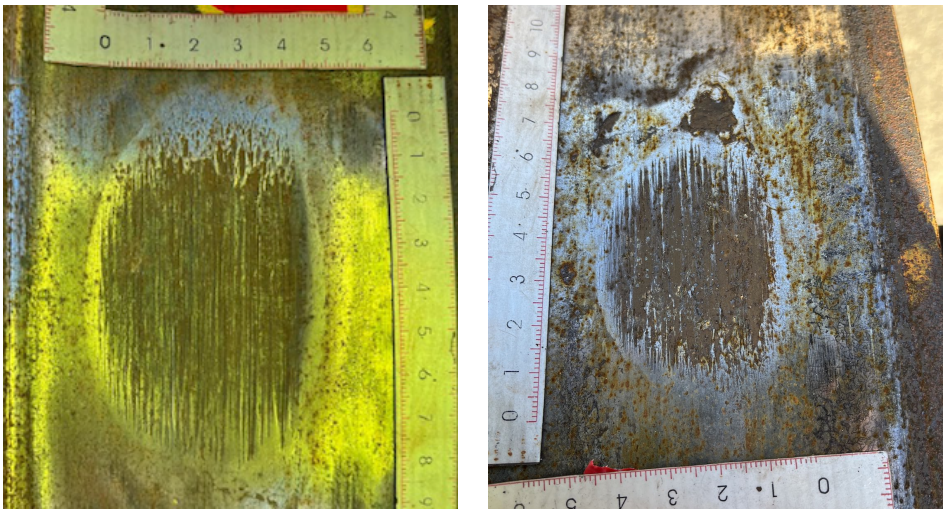

(a) Wheel flat 1

(b) The wheel flat on the other wheel

Figure 4.3: (a) Wheel flat 1 and (b) the flat on the other wheel on the same axle. Picture courtesy: Michele Maglio

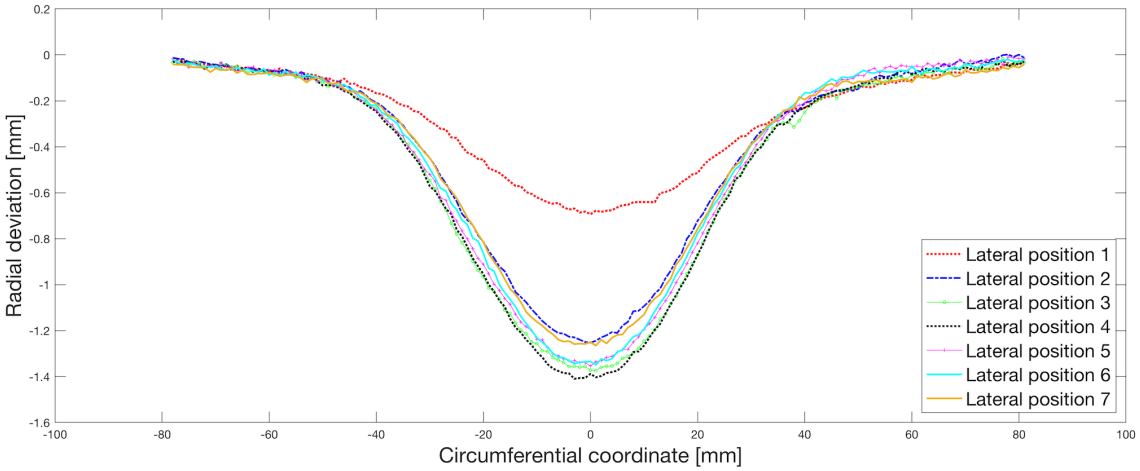

Figure 4.4: Radial deviation of wheel flat 1 from the nominal tread surface at different lateral positions. Since the rounded edges should not be included in the registered flat length, the flat can be assumed to have its maximum length located between the circumferential coordinates -40 and 35 mm. The figure illustrates how the length of the flat varies between the different lateral positions. The depth of the wheel flat is maximum at around 1.4 mm for lateral position 4.

The wagon with this tread damage had been driving in the southern parts of Sweden and had passed through wheel impact load detectors located in Dammstorp, Kumla, Kävlinge, and Bodarne. These are all of the type SCHENCK [6]. Data from these detectors have been collected to be able to compare the results from the simulations to the measured values. From the period of September to November 2021 there were in total 10 passages in detectors, which were the final ones before the wheel was replaced. For the left wheel of the axle, the ratio (peak load divided by mean

load) from most passages is higher than for the right wheel, which leads to the assumption that the left wheel had the 75 mm wheel flat while the length of the flat on the right wheel was 50 mm. The differences in ratio between the two wheels indicate that the wheel flats can have been existing for all those ten passages, even though the dynamic loads are not high enough to be certain. A plot of the ratio for both wheels on the axle is presented in figure 4.5 while additional data for the left wheel is presented in table 4.1.

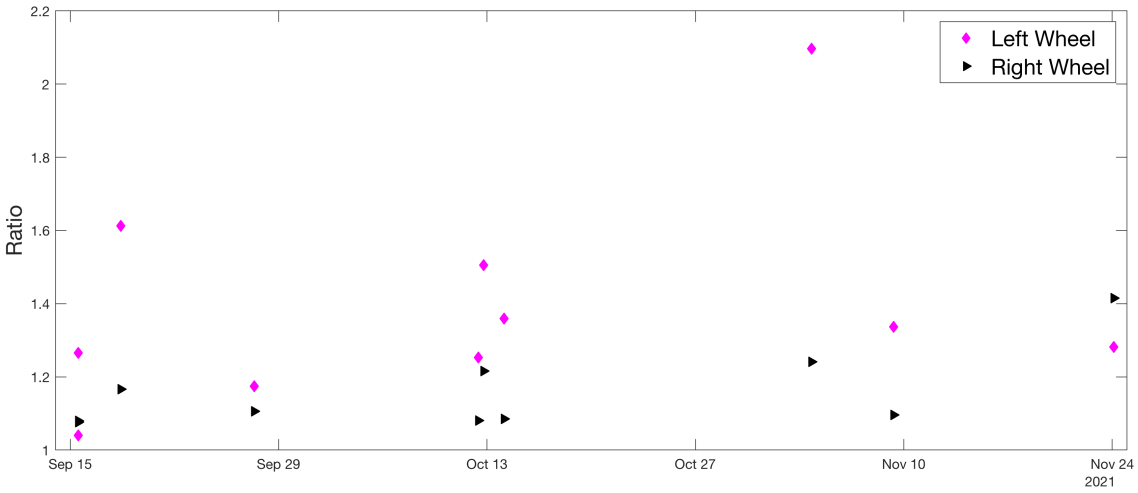

Figure 4.5: Ratio values from the right and left wheels

Table 4.1: Data collected for wheel flat 1 (left wheel on the axle). The axle load was calculated as the mean load of the left wheel multiplied by two.

Axle Load [t]	Peak Load [kN]	Dynamic Load [kN]	Speed [km/h]	Detector location
20.4	104	4	75	Dammstorp USP
23.0	143	30	75	Dammstorp USP
6.3	50	19	104	Kumla USP
21.0	121	18	75	Dammstorp NSP
19.4	119	24	31	Kävlinge ESP
19.0	140	47	96	Bodarne USP
18.1	121	32	86	Kumla USP
6.3	65	34	100	Kumla USP
21.8	143	36	87	Dammstorp NSP
15.9	100	22	86	Dammstorp USP

4.2 Wheel flat 2 - 120 mm

The second wheel tread damage is named "wheel flat 2". It is a wheel flat with a length of 120 mm, and a maximum depth of 1.2 mm, see figure 4.6a. This means that compared to wheel flat 1, this wheel flat is longer but less deep. The characteristics

of the shape do not agree with what would be expected according to the chord theorem [35], where the chord of the circle (the length of the wheel flat) can be calculated by knowing the intersection point (depth of the flat) and the diameter. According to this formula, a depth of 1.2 mm of the flat would correspond to a flat length of 65 mm, assuming a wheel diameter of 0.88 m. Figure 4.7, however, confirms that the shape of the damage has a geometry that resembles one long flat. The reason for the odd geometry is unknown but can be due to reasons such as a worn rail profile where the flat was created. Another reason, and probably the more likely one, could be that the edges of the flat have been worn off substantially and look like they are a part of the flat. Thus, initially, the flat might have been shorter than 120 mm. The other wheel on the axle also had a flat, see figure 4.6b, whose length is hard to distinguish from the picture as it seems to continue under the white measuring tape. The wheel was scanned in March 2018, and seven detector passages have been found, presented in table 4.2. The RFID technology was not used in these passages in 2018, which leads to greater uncertainty regarding if the data comes from the right wagon. To double-check this, the mean load (axle load) from the detectors has been compared with the history of registered weights of the wagon which was located in a Green Cargo train. The outcome was that the load measured in the detectors showed a good agreement with the registered weight of the wagon.

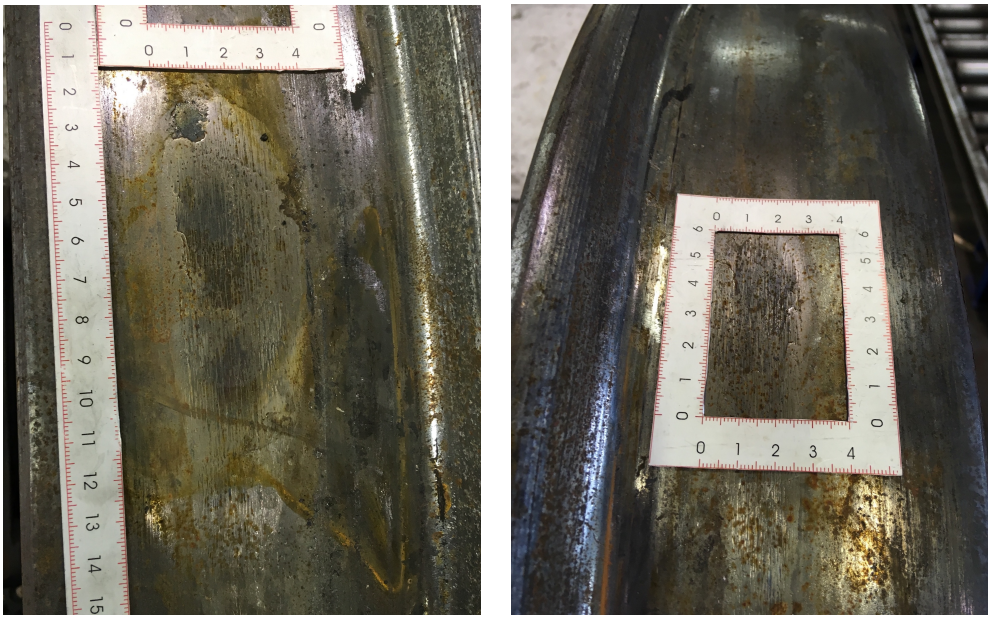

(a) Wheel flat 2

(b) The wheel flat on the other wheel

Figure 4.6: (a) Wheel flat 2 and (b) the flat on the other wheel on the same axle. Picture courtesy: Michele Maglio

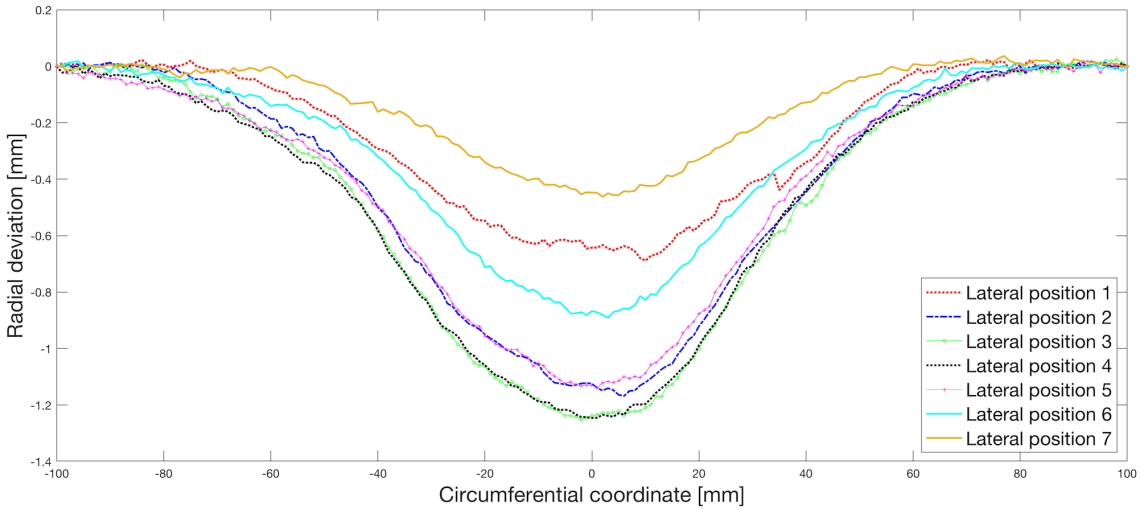

Figure 4.7: Radial deviation of wheel flat 2 from the nominal tread surface at different lateral positions. The wheel flat is assumed to start at the circumferential coordinate -60 mm and continue to 60 mm, which gives a 120 mm length of the wheel flat.

Table 4.2: Data collected for the axle with wheel flat 2. It is not known if wheel flat 2 is located on the left or right wheel. The axle load is calculated as the mean load of each wheel multiplied by two. The detector locations in order from top to bottom: Krokvik, Lappberg, Harrträsk, Vassijaure, Vassijaure, Koler, Mellansjö NSP. The detector in Mellansjö NSP is of the type "PHOENIX MDS WILD", while the rest are of the type "SCHENCK".

Left Wheel				Right Wheel			
Axle Load [tonnes]	Peak Load [kN]	Dynamic Load [kN]	Speed [km/h]	Axle Load [tonnes]	Peak Load [kN]	Dynamic Load [kN]	Speed [km/h]
10.0	123	74	99	12.6	181	119	99
11.2	91	36	97	11.8	212	154	97
11.2	153	98	76	11.2	234	179	76
12.2	106	46	81	10.4	197	146	81
9.4	89	43	81	6.9	165	131	81
7.3	113	77	73	7.3	217	181	73
8.4	82	41	76	8.0	141	102	76

4.3 Geometric difference between wheel flats 1 and 2

The geometric difference between wheel flats 1 and 2 is presented in figure 4.8. The lateral position with the maximum depth was chosen, which was position 4 for both wheel flats. The figure shows that the gradient in radial deviation at the edges of wheel flat 1 is significantly greater than for wheel flat 2.

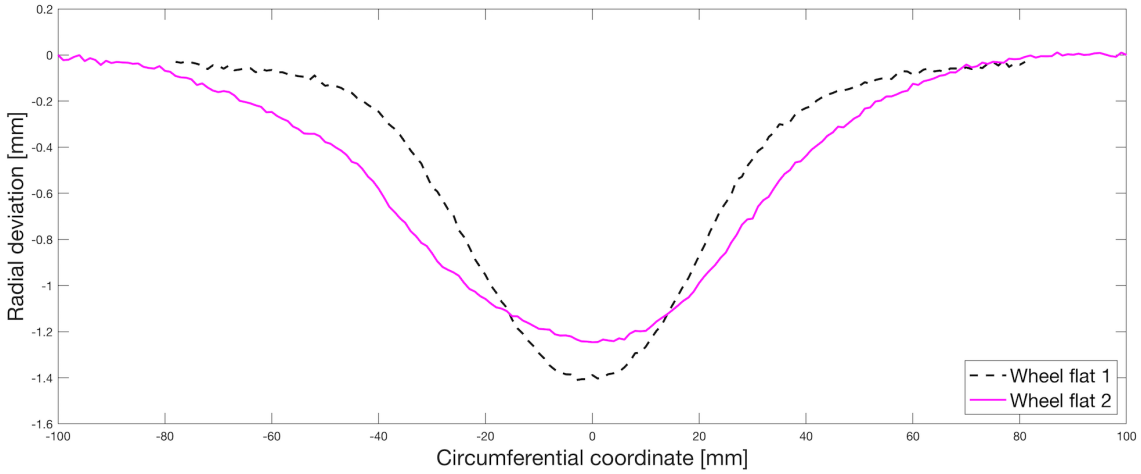

Figure 4.8: The radial deviation for the maximum depth of wheel flats 1 and 2 demonstrated in the same figure.

5

Simulation of wheel-rail impact loads

To simulate wheel-rail impact loads, the in-house-software WERAN was used. The simulations analyze how the wheel flat geometry, train speed, axle load, lateral contact positions, and unsprung mass influence the impact load.

5.1 Introduction

To understand how the unsprung mass influences the peak loads generated by wheel flat 1, the simulations will be performed with both a new wheel (non-reprofiled with a diameter of 0.92 m) and a wheel reprofiled to its minimum diameter (0.84 m). The mass of the non-reprofiled wheelset is 1137 kg while the wheelset with reprofiled wheels weighs 904 kg. Thus the difference in the unsprung mass between the simulations is 233 kg. In addition to this, the simulations aim at understanding how train speed and axle load influence the generated load, therefore the following simulation cases were studied:

- Constant train speed of 100 km/h and varying axle load between 5-25 tonnes
- Constant axle load of 25 tonnes and varying speed between 40-140 km/h
- Constant axle load of 5 tonnes and varying speed between 40-140 km/h (only for wheel flat 1)

To investigate the influence of impact position within a sleeper bay, the simulation is performed so that the wheel flat will hit the rail eight times in different equidistant positions over the sleeper bay, see figure 5.1. Since a wagon can move in two directions, the wheel flat was also introduced to hit the rail in both directions. Even though the length of the flat will be the same, the geometry of the flat might not be symmetric with respect to its centre and therefore both directions will be simulated for all the cases above. This means that the result from each combination of axle load, speed, and lateral contact position will be based on 16 wheel-rail impact cases. To quantify the effect of where in the sleeper bay the wheel flat hits the rail, the mean, standard deviation, and maximum of the 16 impact loads will be presented.

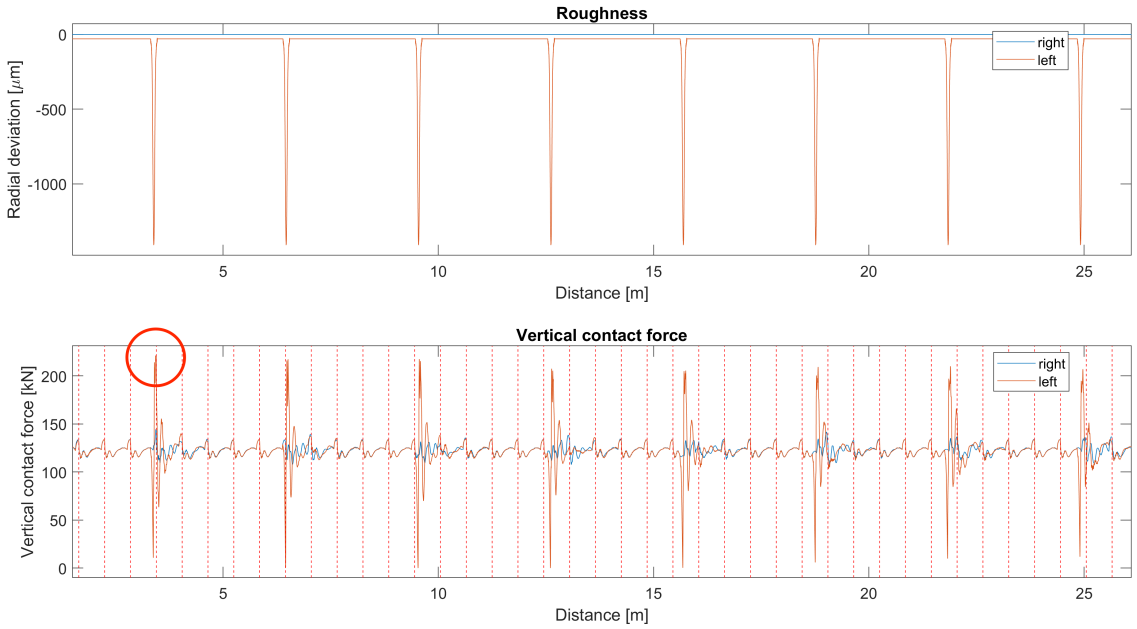

Figure 5.1: An example showing simulated results for wheel flat 1 in WERAN, speed 90 km/h, axle load 25 tonnes, and lateral contact position 4. The variation in wheel radial deviation of the rolling contact is indicated in the top figure, where the dip due to the wheel flat occurs eight times, which is the number of times the wheel flat hits the rail in the simulation for each traffic direction. In the bottom figure, the time history of the vertical wheel-rail contact force is presented. The dashed orange lines illustrate the positions of the sleepers, with 0.6 m spacing between each one. As expected, the vertical force has a higher magnitude when the wheel flat hits the rail above the sleeper, (indicated by the red circle), than between sleepers.

The wheelset type which has been used in all simulations is 57H. Wheel flats 1 and 2 were 3D-scanned from the wheelset types 59H and 57H respectively. In the simulations, the surface of each of these defects was then superposed on a nominal 57H wheel surface. The 59H wheelset type is assumed to be similar enough to the 57H so that it is reasonable to compare the data from detectors with the simulation results. Table 5.2 below summarizes the rail and sleeper properties used in the simulations for the track model. The same properties as in [36] have been adopted.

Figure 5.2: The rail and sleeper properties used for the track model, source: [36].

Table 1
Sleeper and rail properties used in the track model.

	Sleeper	Rail
Reference model	Abetong A22 sleeper	60E1 rail
Young's modulus (GPa)	37.5	210
Poisson's ratio	0.20	0.30
Density (kg/m^3)	2400	7800
Shear factor	0.845	0.40
Cross-sectional area (m^2)	$5.44 \bullet 10^{-2}$	$7.69 \bullet 10^{-3}$
Moment of inertia (m^4)	$2.12 \bullet 10^{-4}$	$3.05 \bullet 10^{-5}$

Further, the sleeper support bed modulus is 100 kN/m^3, and the corresponding viscous damping per unit area 82 kNs/m. Rayleigh damping is assumed for the wheelset with scale factor 50 for the mass proportional damping and 7e-6 for the stiffness proportional damping.

5.2 In-house software WERAN

To simulate vertical dynamic wheel-rail contact forces, the in-house MATLAB software WERAN (WheEl/RAil Noise) has been used. Information about the development of the program and the theory used can be found in [37]. The first step was that 3D FE models were created for the track and wheelset, Figure 5.3 illustrates the wheelset model. To simulate both a non-reprofiled wheel and a reprofiled wheel, two different models have been used. These models make it possible to obtain the frequency response functions, which are acquired for both the wheelset and track models. Figure 5.4 presents the frequency response functions for the wheelset.

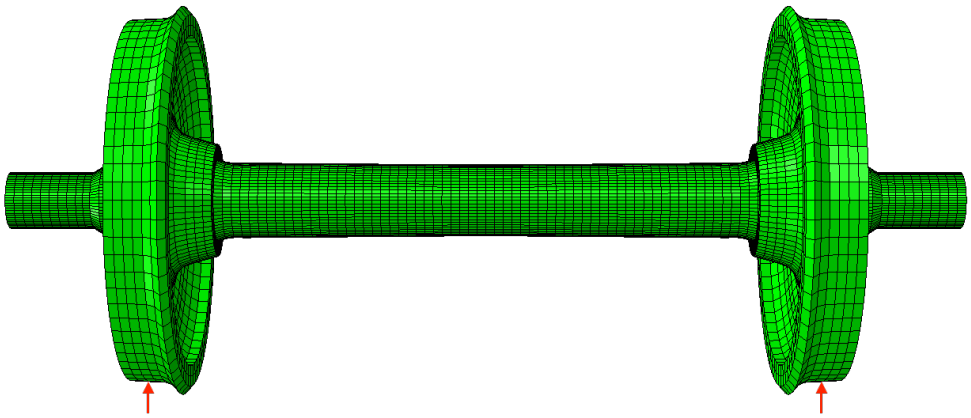

Figure 5.3: 3D FE model of the wheelset, the contact points on the wheel are illustrated by the red arrows

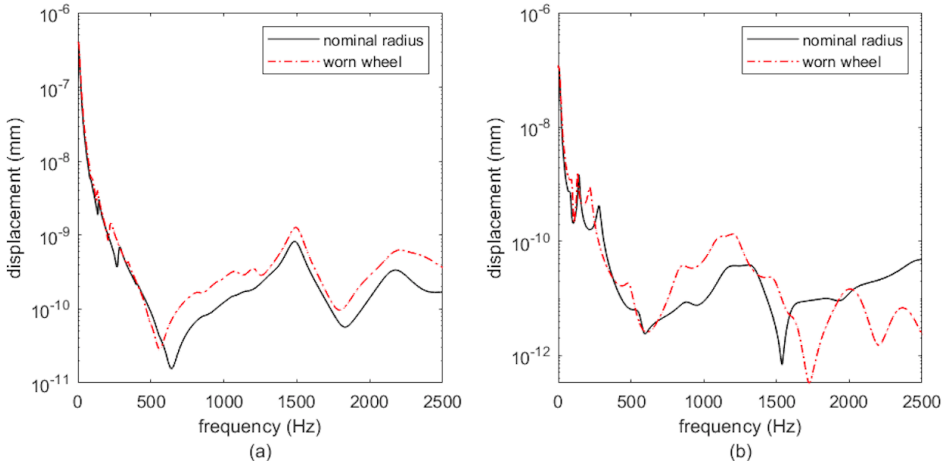

Figure 5.4: The frequency response functions for the nominal wheel-rail contact point on a non-reprofiled (nominal radius) or reprofiled wheel (worn wheel).
(a) Direct receptance when the load is applied on the same contact point
(b) Cross receptance when the load is applied on the contact point on the opposite wheel

The program performs simulations in the time domain with the help of Green's functions. These are used to model the track and wheelset dynamic response and are based on the frequency response functions, see [32]. Cross receptances $R^W_{i,j}(f)$ and the corresponding Green's function $G^W_{i,j}(t)$ are also considered to include the influence of interaction between the two wheels via the axle and via the track. The Green's functions for the wheelset $G^W_{i,j}(t)$, are calculated by using the inverse Fourier transform.

$$G^W_{i,j}(t) = \mathcal{F}^{-1}(R^W_{i,j}) \tag{5.1}$$

The Green's functions for the wheelset is presented in figure 5.5.

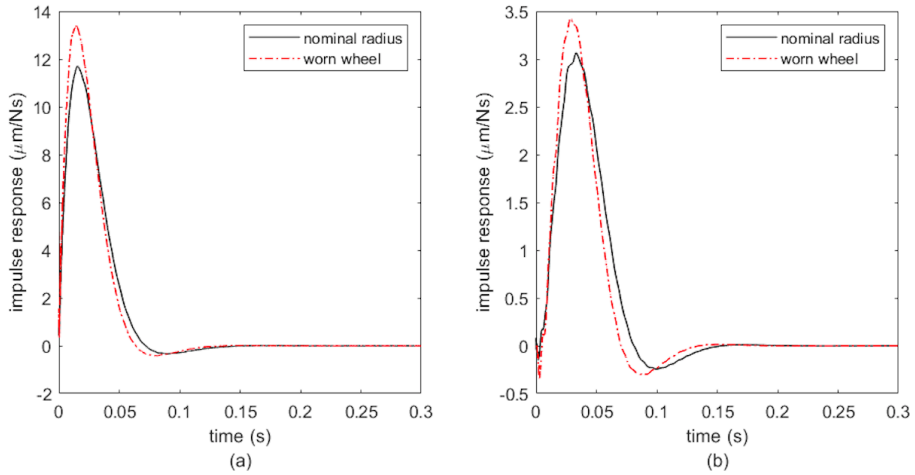

Figure 5.5: The Green's functions for the nominal wheel-rail contact point on a non-reprofiled (nominal radius) or reprofiled wheel (worn wheel).
(a) When the load is applied on the same contact point
(b) When the load is applied on the contact point on the opposite wheel

In [32], it was shown that the cross-coupling between the wheels is rather weak by studying a wheelset with one damaged wheel and one without defects. Since the wheelset's rotation is not accounted for in WERAN, the Green's function corresponds to the impulse response of the radial displacement. Further, the relative longitudinal motion between the wheelset and the track needs to be considered. This is done by developing so-called moving Green's functions for the track, which need to be calculated separately for each considered train speed. This enables to consider varying train speeds in combination with different axle loads. Figure 5.6 shows an example of a moving Green's function, from [36].

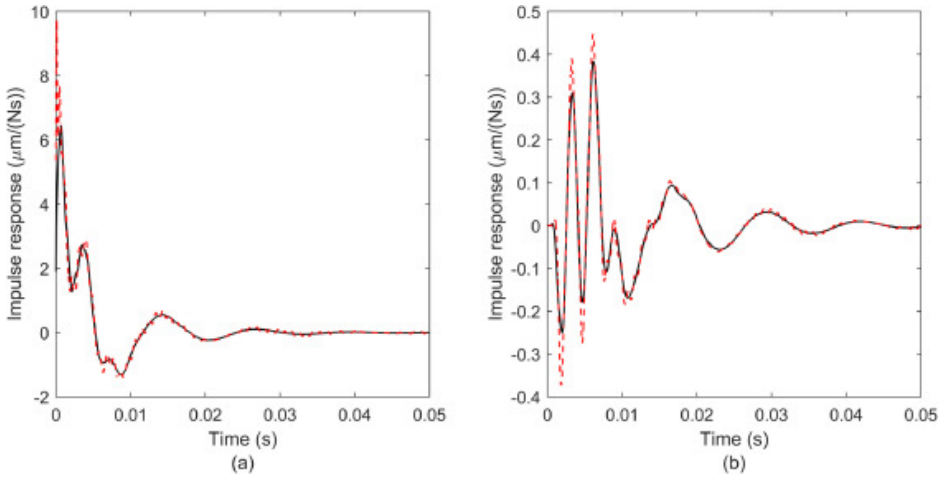

Figure 5.6: The moving Green's functions for the track at train speed 100 km/h from [38]. The black line illustrates the function for the load on top of a sleeper, and the red dashed line in the middle of a sleeper bay.
(a) When the load is applied on the same rail
(b) When the load is applied on the opposite rail

The wheel-rail contact is solved by using Kalker's variational method. The program defines a potential contact patch which is discretised in a mesh of 1 mm^2 elements. For each mesh element and for each time step, the program computes the pressure between the wheel and rail as well as the distance between the wheel and rail surfaces using an iterative procedure. During this iteration, deviations from the nominal wheel and rail geometries are accounted for. In this work, the deviations from the nominal wheel geometry for different lateral positions on the two studied defects (see figures 4.4 and 4.7) are accounted for. From these results, the contact forces and the vertical displacement of the wheel and the rail can be calculated. The sampling frequency adopted in the in-house software WERAN depends on the simulated vehicle speed and is determined by the time interval required by the vehicle to cover a distance of 1 mm at the given speed. For example, at 100 km/h, the sampling frequency is around 27.8 kHz

5.2.1 Verification of WERAN

A verification of the theory used in WERAN was carried out in [39], where both a newly formed and a rounded wheel flat were modelled and simulated. The verification was then made by comparing the computed results to the result of the field test which was mentioned in section 2.3 and presented in figure 2.4 [13]. It was concluded that the encouraging level of agreement between the calculated result and the field test result establishes that the modelling approach is functioning. It is further discussed in [37] that the level of agreement is encouraging, especially considering the challenge of characterizing the test site and track parameters. Another verification was made in [38] where a damaged wheel was studied in a field test by running it through a wheel impact load detector at different speeds. The wheel, which had been affected by wear on a big part of the tread as well as rolling contact fatigue clusters, was then scanned. A comparison of the vertical peak impact loads was then made, taking several parameters into consideration, such as speed. Good agreement between the simulated result and the measured data was obtained, especially at a vehicle speed of 100 km/h.

5.3 Wheel flat 1 - 75 mm

The first wheel flat which was presented in chapter 4, named "Wheel flat 1", has been simulated in WERAN and the results are presented below. The maximum peak load is the highest load based on the 16 times the wheel flat hits the rail during each pair of simulations (two different traffic directions). In Appendix B, the mean for those 16 peak loads is presented, along with their standard deviation.

5.3.1 Constant train speed at 100 km/h - varying axle load

The figures below present how the maximum peak load is dependent on the axle load and unsprung mass. Figure 5.7, presents the results for a wheel with nominal (maximum) wheel diameter 0.92 m and maximum unsprung mass. Figure 5.8 presents the corresponding results for a wheel that has been reprofiled to its minimum diameter at 0.84 m.

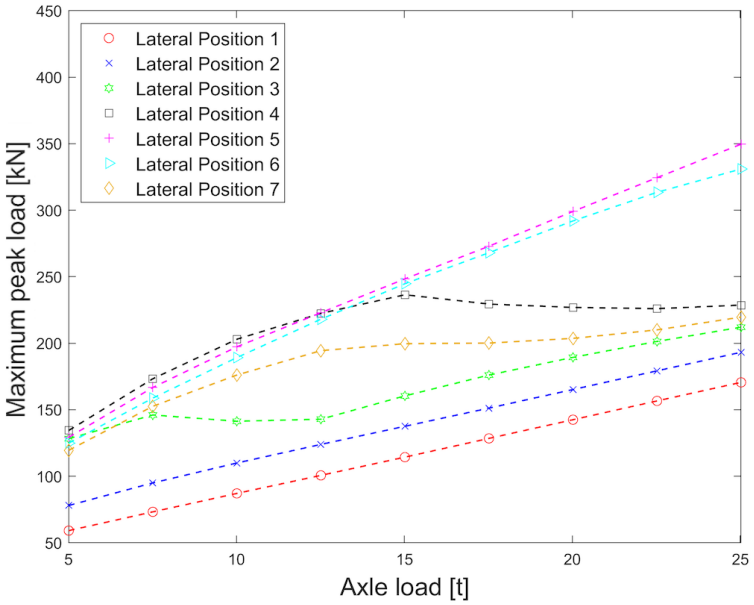

Figure 5.7: Wheel flat 1: influence of lateral contact position and axle load on maximum peak load. Nominal wheel diameter 0.92 m and train speed 100 km/h.

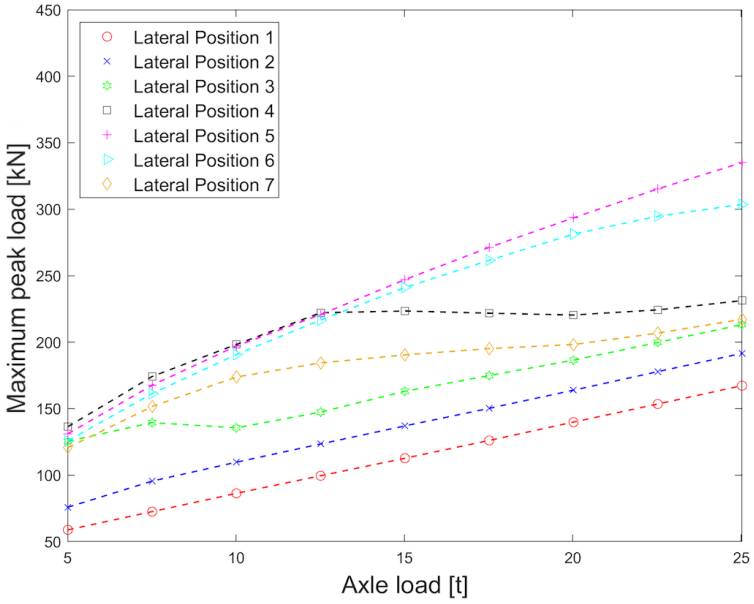

Figure 5.8: Wheel flat 1: influence of lateral contact position and axle load on maximum peak load. Reprofiled wheel (diameter 0.84m) and train speed 100 km/h.

For the nominal wheel, it is observed that the alarm limit 350 kN is reached at around 25 tonnes axle load. The reprofiled wheel with lower unsprung mass is close but never reaches 350 kN in the simulation. What can be noticed, however, is that the difference between the two simulation cases is not so significant, meaning that the influence of the unsprung mass is relatively small. The highest peak loads were obtained for lateral contact position 4 at lower axle loads and for lateral position 5 at higher axle loads.

5.3.2 Constant axle load at 25 tonnes - varying train speed

Figures 5.9 and 5.10 present how the maximum peak load is dependent on the train speed and unsprung mass. From chapter 3 it is known that trains with loaded wagons operate between the train speeds 64–90 km/h and unloaded 69–120 km/h.

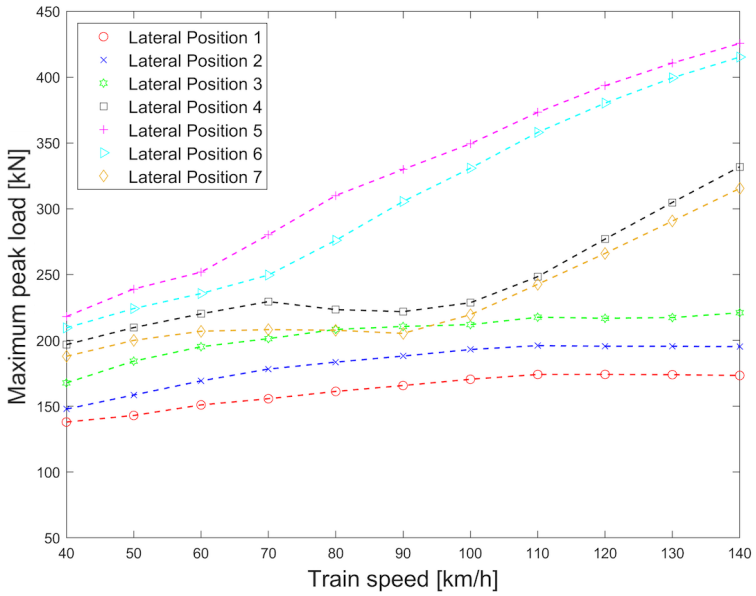

Figure 5.9: Wheel flat 1: influence of lateral contact position and train speed on maximum peak load. Nominal wheel diameter 0.92 m and axle load 25 tonnes.

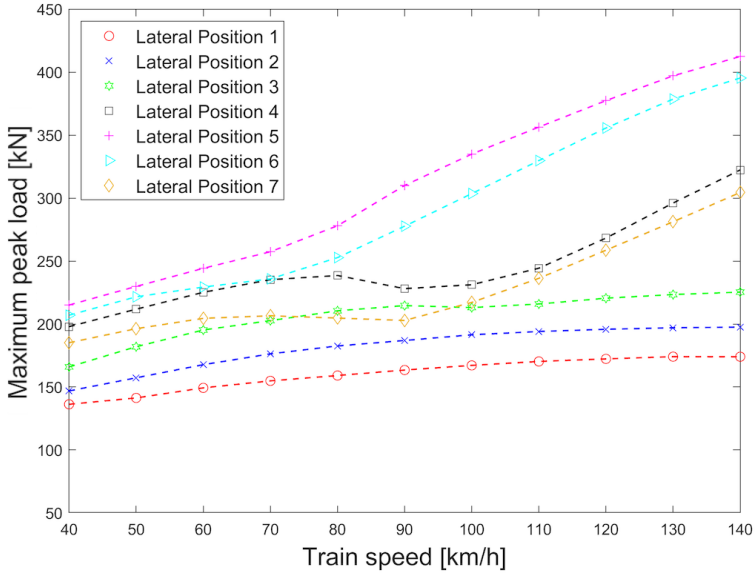

Figure 5.10: Wheel flat 1: influence of lateral contact position and train speed on maximum peak load. Reprofiled wheel (diameter 0.84) m and axle load 25 tonnes.

Also in this case, the results from the simulations show that the influence of the unsprung mass is relatively small in relation to the magnitude of the forces. The peak

load of 350 kN is reached at 100 km/h for the wheel which has not been reprofiled. In the literature review, a local maximum in the wheel-rail impact forces could be seen at around 40 km/h, see figure 2.4. The simulations above do not show a similar trend, however, a local maximum can be seen for some lateral contact positions at around 70-80 km/h. Other lateral positions indicate almost a linear relation with train speed. In general, the contact forces increase very differently depending on the lateral contact position in the interval 40–140 km/h.

5.3.3 Constant axle load at 5 tonnes - varying train speed

Simulations with a constant axle load of 5 tonnes have been performed to be able to simulate the case of an unloaded wagon. The results can be compared with the case of a loaded wagon in figure 5.9 (axle load 25 tonnes). As expected the peak loads are much lower for this lower axle load. Interestingly, for the lateral position leading to the highest peak loads, the maximum peak loads are very similar for speeds higher than 70 km/h.

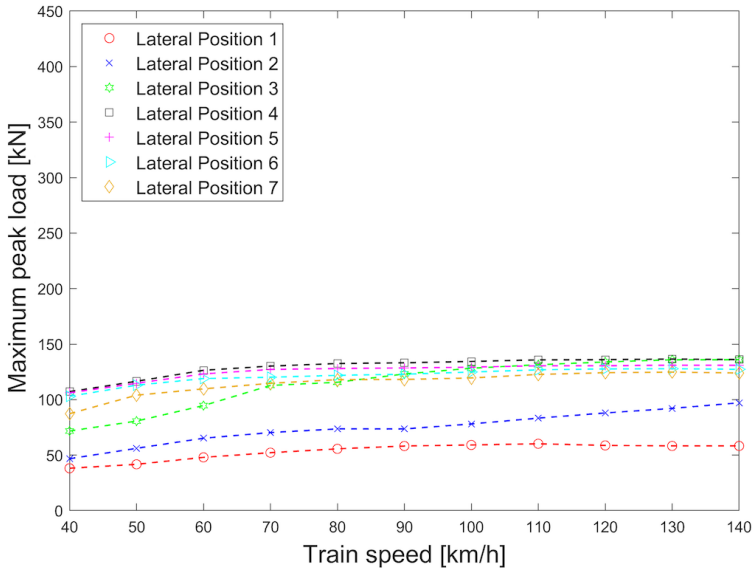

Figure 5.11: Wheel flat 1: influence of lateral contact position and train speed on maximum peak load. Nominal wheel diameter 0.92 m and axle load 5 tonnes

5.3.4 Maximum peak loads for wheel flat 1

As can be noticed in the figures above, lateral contact position 5 overall leads to the highest magnitudes of peak loads. This position was therefore chosen to further illustrate and summarise the influence of train speed and axle load on maximum peak load. Figure 5.12 presents the maximum peak loads, for the wheel with nominal diameter (0.92 m) while evaluating all 16 possible impact positions (8 positions within a sleeper bay and two traffic directions). The non-reprofiled wheel was chosen as the unsprung mass is the highest and therefore gives the most conservative simulation results in terms of peak loads. The corresponding dynamic loads are presented in

appendix B, see figure B.5, and it is observed that the magnitude of the dynamic load increases with increasing axle load and train speed.

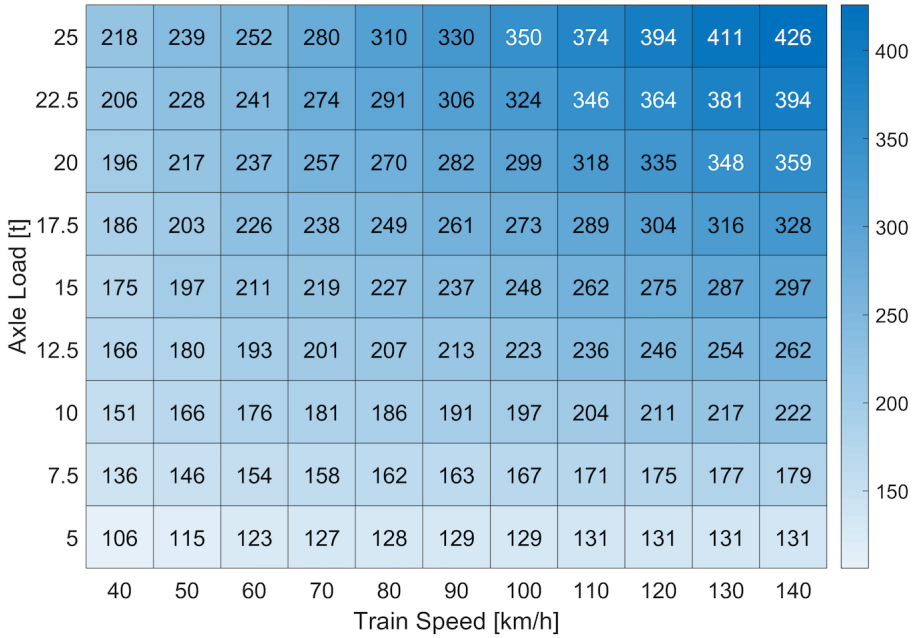

Figure 5.12: Wheel flat 1: influence of train speed and axle load on the maximum peak load expressed in kN. The highest peak loads are obtained for high axle loads in combination with high train speed. Lateral contact position 5.

Some values in figure 5.12 exceed 350 kN. These are, however, not for combinations of train speed and axle load that are used in normal driving conditions. From the analysis of the detector data it was clear that the loaded wagons did not exceed a train speed of 90 km/h.

5.4 Wheel flat 2 - 120 mm

Since the unsprung mass did not show a big influence in terms of peak loads, see section 5.3.2, wheel flat 2 was only simulated for the non-reprofiled wheel. Note that the scale of the vertical axis, describing the maximum peak load, has been changed compared to wheel flat 1 since the magnitudes of the contact forces are significantly lower.

5.4.1 Constant train speed of 100 km/h - varying axle load

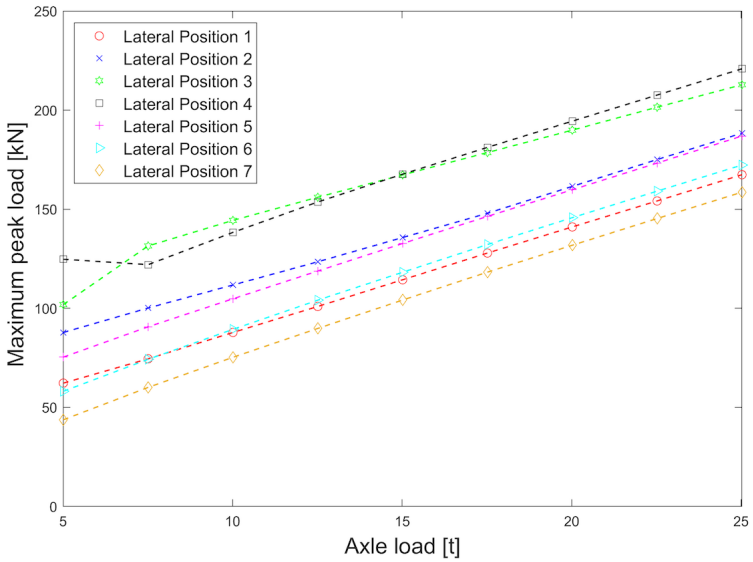

Figure 5.13: Wheel 2 simulated with a constant train speed of 100 km/h

As can be seen in figure 5.13, the increase depending on the axle load shows a relatively linear behaviour. The peak loads are significantly lower compared to wheel flat 1, cf. figure 5.7, and are not even near to reach the warning alarm of 280 kN.

5.4.2 Constant axle load of 25 tonnes - varying train speed

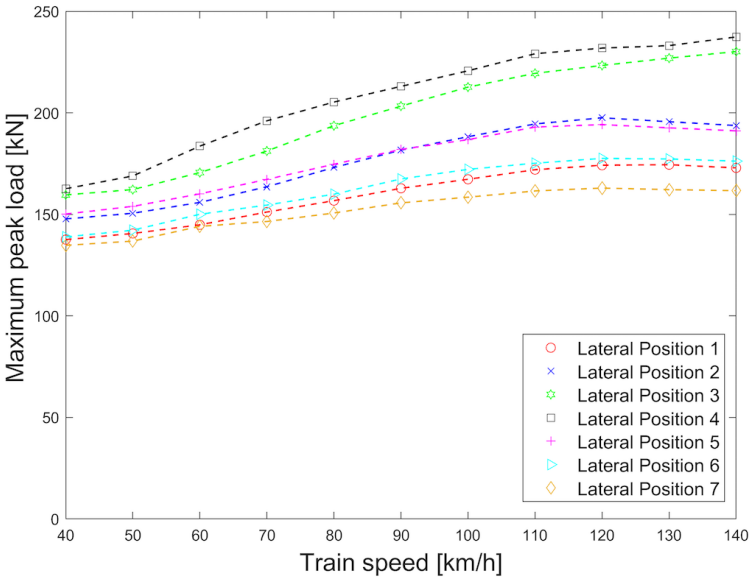

Figure 5.14: Wheel 2 simulated with a constant axle load of 25 tonnes

As can be seen in figure 5.7, the shape of the increase depending on train speed is varying for different lateral positions as for wheel flat 1. A local maximum around 120 km/h can be seen for some lateral positions. This local maximum is at a higher speed compared to the literature review and the results from wheel flat 1. The reason for this is probably the longer total length of the radial deviation from the nominal surface of the wheel tread.

The resulting peak loads from wheel flat 2 are significantly lower than for wheel flat 1, even though the wheel flat has a longer length. The fact that the flat is less deep can explain the difference, but also the gradient in radial deviation at the edges of the flat which is smaller compared to wheel flat 1. This implies that the edges of wheel flat 2 may have been rounded off to a bigger extent. Due to these lower forces, simulations have not been carried out for axle load 5 tonnes for wheel flat 2.

5.4.3 Maximum peak loads for wheel flat 2

According to figures 5.13 and 5.14, lateral position 4 was the one that gave the highest peak loads for wheel flat 2, which is why it was chosen for further investigation for additional speeds and axle loads. The influence of train speed and axle load on maximum peak load is presented in figure 5.15. In general, cf. figure 5.12, it is observed that peak loads are increasing with increasing speed and axle load. The dynamic loads are presented in a corresponding figure in Appendix B, see figure B.6. In figure B.6, it is observed that the influence of axle load on dynamic load is relatively weak. However, a maximum dynamic load is obtained at axle load 7.5 tonnes, which is a different observation compared to wheel flat 1, cf. figure B.5, where the influence of axle load was more significant and the highest dynamic load was obtained for the maximum axle load. For both wheel flats, the dynamic load increases with increasing train speed.

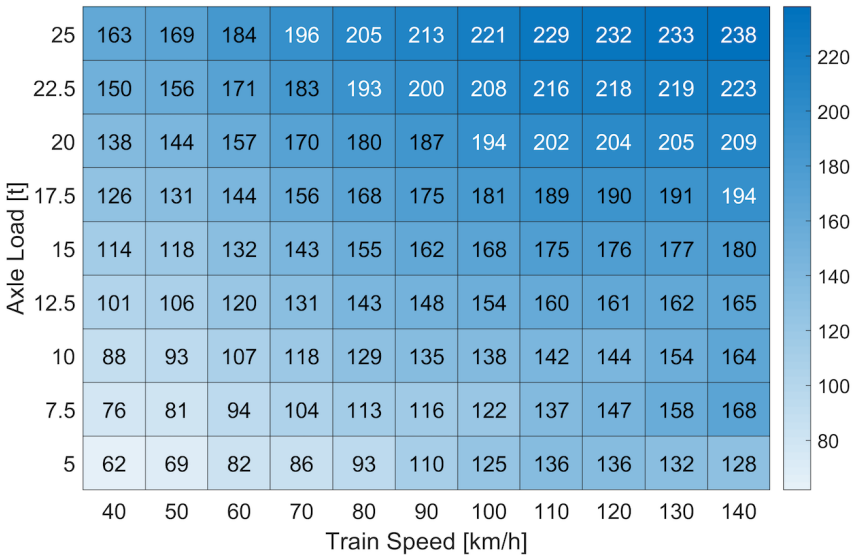

Figure 5.15: The maximum peak load expressed in kN for wheel flat 2: lateral contact position 4.

6

Comparison between detector data and simulation results

The analysis of detector data in chapter 3 considered different intervals of flat lengths which makes it possible to compare the results from the detector analysis with the simulated results for wheel flats of corresponding lengths. The simulation results are partly presented in appendix B (B.1 - B.4), showing the mean and standard deviation of the peak loads from different hit positions in the sleeper bay. Those values are lower than the maximum peak loads presented in the figures in chapter 5. It is argued that the mean value provides a better representation of what on average would be observed in a detector since it in a way reflects the expected trend in measured loads for a wheel flat in a given length interval striking the detector at different positions. Figure 6.1 compares the results from the analysis made of the detector data for flat lengths 70–79 mm in the loaded case, with the simulated results for wheel flat 1. Based on the scatter in measured data in figure 6.1a, a red box is inserted on the vertical axis between 125–300 kN and for the relevant speeds and axle loads. The result shows that the simulated value of wheel flat 1 has a good agreement with the values of the same flat length from the detectors. This is stated because the box covers almost all detector passages as well as the peak loads from different lateral positions.

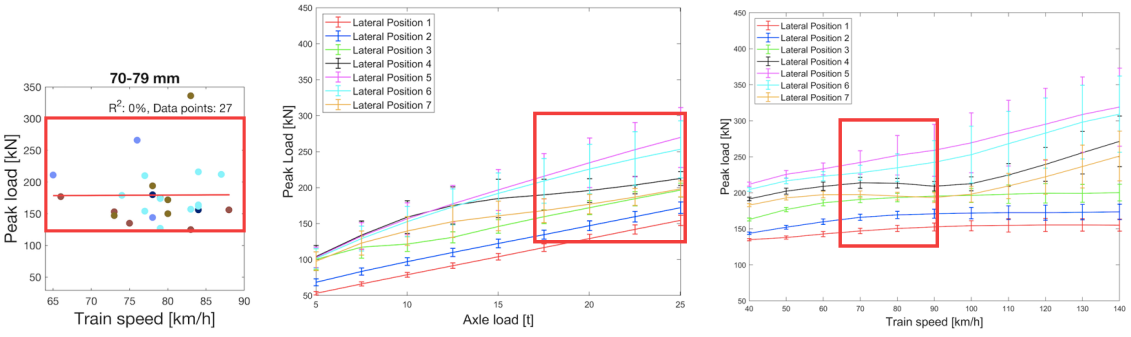

(a) Axle loads of 17-25 tonnes

(b) Constant train speed at 100 km/h

(c) Constant axle load at 25 tonnes

Figure 6.1: Comparison between the analysis of the detector data presented in figure 3.5 and the results from the simulations presented in figures B.1 and B.2 .

The axle with wheel flat 1 passed through ten wheel impact load detectors as presented in table 4.1, allowing for an additional comparison between these measured

data and the simulated results. Not all values are possible to compare, since the axle load and train speed do not match. However, here train speeds above 80 km/h from the detectors passages are used for comparison with the values simulated for 100 km/h, and axle loads above 21 tonnes from the detectors are compared to 25 tonnes in the simulations. This can affect the comparison since a lower axle load and train speed in most cases results in a lower peak load. It should be mentioned that the wheel flat has been assumed to have been generated before all the detector passages, which was discussed in chapter 3, however, this can be considered as an uncertainty.

Axle Load [t]	Peak Load [kN]	Dynamic Load [kN]	Speed [km/h]
20.4	104	4	75
23.0	143	30	75
6.3	50	19	104
21.0	121	18	75
19.4	119	24	31
19.0	140	47	96
18.1	121	32	86
6.3	65	34	100
21.8	143	36	87
15.9	100	22	86

(a) The detector data from wheel flat 1

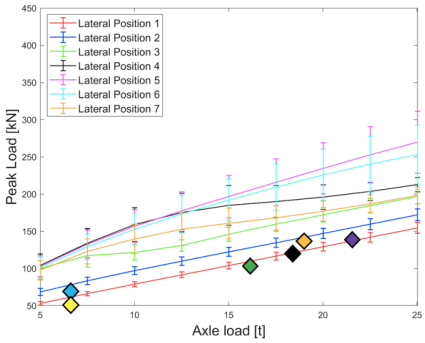

(b) Constant train speed at 100 km/h

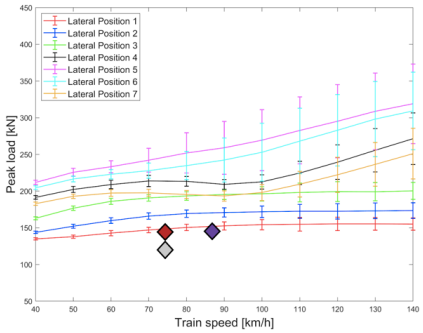

(c) Constant axle load at 25 tonnes

Figure 6.2: Comparison between the detector data from wheel flat 1 previously presented in table 4.1. The detector values which can be compared to the simulated values are marked by different colors next to the detector value and inserted in figures 6.2b and 6.2c

It is concluded that the data collected from the wheel impact load detectors are of the same order of magnitude, or slightly lower, as the simulation results for the lateral positions which gave rise to the lowest impact loads. As mentioned, the combinations of axle load and train speed are generally lower for the detector data compared to the simulations, which is one reason why the detector values have lower peak loads. Other influencing parameters can be uncertainties and differences in how the sensor data are post-processed compared to the simulation, calibration of the detectors for high-frequency dynamic loads as well as various input parameters in

the simulations such as the track stiffness.

The same comparison has been carried out for the results from wheel flat 2. For this flat, it is not clear if wheel flat 2 was located on the left or the right wheel of the axle, which is why both wheel's detector data are included in the analysis. Since the detector data presented in chapter 3 for flat lengths of 120 mm were few, the simulated values are only compared to its own detector data. Due to having no values of axle loads close to 25 tonnes axle load, only a comparison was made with the simulation with varying axle loads. Just like in the comparison with wheel flat 1, train speeds above 80 km/h have been compared with simulation results performed for train speed 100 km/h.

Left Wheel			
Axle Load [tonnes]	Peak Load [kN]	Dynamic Load [kN]	Speed [km/h]
10.0	123	74	99
11.2	91	36	97
11.2	153	98	76
12.2	106	46	81
9.4	89	43	81
7.3	113	77	73
8.4	82	41	76

(a) The detector data for the left wheel

Right Wheel			
Axle Load [tonnes]	Peak Load [kN]	Dynamic Load [kN]	Speed [km/h]
12.6	181	119	99
11.8	212	154	97
11.2	234	179	76
10.4	197	146	81
6.9	165	131	81
7.3	217	181	73
8.0	141	102	76

(b) The detector data for the right wheel

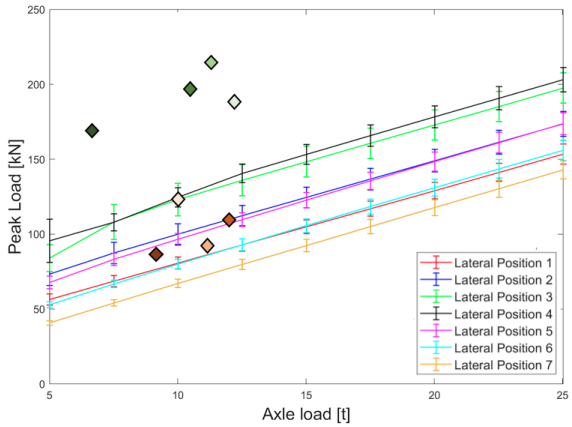

(c) Constant train speed at 100 km/h

Figure 6.3: Comparison between simulation and the detector values for wheel flat 2 which was originally presented in chapter 4.2. The detector values which can be compared to the simulated values are marked by different colors next to the detector value and inserted in figure 6.3c

Figure 6.3 shows that the detector values for the left wheel have a good agreement with the simulations since all data are in the range of the different lateral positions. The right wheel, on the other hand, has detector values that all exceed the simulated loads. This implies that the scanned geometry of wheel flat 2 was located on the left wheel.

6.1 Additional comparison to literature review

In the literature review, see chapter 2, figure 2.3 illustrated the influence of wheel flat length on simulated peak load. The axle load was 30 tonnes and the speed 60 km/h. The results from the referenced paper, [25], showed that peak load 350 kN was reached at a flat length of approximately 113 mm, and with the formula provided in the paper, that corresponded to a depth of 1.6 mm. That flat is deeper than the flats considered in the simulations in this paper, where wheel flats 1 and 2 had a depth of 1.4 mm and 1.2 mm, and those two cases showed a great difference in the impact loads. The results from this thesis seem to be reasonable compared to the results in reference [25].

In the field tests at Svealandsbanan and Sannahed, the peak loads for axle loads of 9, 21, and 24 tonnes and train speed interval 10-100 km/h were consistently below 250 kN. For 21 and 24 tonnes axle load, a local maximum in peak load was obtained around 40 km/h. The results from the simulations in the present report do not indicate a local maximum around this speed. For wheel flat 1, a local maximum can however be seen at around 70 km/h for some lateral contact positions. For wheel flat 2, there is a local maximum in peak load for some lateral positions at around 120 km/h. The flat from Svealandsbanan was 100 mm long with a depth of 0.9 mm. Compared to the simulated peak loads for wheel flat 1, which is shorter but deeper, the simulated peak loads overall exceed the results from the field tests. Wheel flat 2 is longer and deeper, but the simulated peak loads show smaller values than the field test for velocities under 70 km/h. This could be due to the geometry of wheel flat 2, which has rounded edges, and also the gradient of the radial deviation is smaller compared to wheel flat 1.

7

Conclusions and recommendations

Based on the analysed detector data, it was not possible to conclude a clear correlation between increasing flat length (or increasing train speed) and increasing peak load. This can be due to several reasons. As discussed in this thesis, and demonstrated in the simulations, the influence of lateral offset between the rolling circle and the centre of the wheel flat on the generated impact load is significant. The same is true for the influence of the position of the impact within the sleeper bay where higher peak loads are generated above or near the sleepers. Further, the simulations showed that the influence of the shape and depth of the flat is more important than the flat length. It is therefore reasonable to assume that one of the reasons for the big scatter in detector data can be that the impact positions are unknown. The fact that the depth of the flat is essential for the resulting forces was confirmed by the literature review. Due to seeing no clear correlation between an increasing flat length and increasing peak load, there are no findings in the present thesis that support the approach used in Trafikverket's regulation restricting the maximum allowed flat length to 60 mm. In addition to this, there were no peak loads from the analysis of detector data (823 samples) or the simulated values that exceeded 350 kN under normal driving conditions even for flats significantly longer than 60 mm.

Based on figures 3.9-3.11, where the passing of a given wheel flat was studied in several detectors along the same southbound (loaded wagons) or northbound (unloaded wagons) journey, it was possible to see how different detectors registered significantly different loads for the same flat. In figure 3.9, it was possible to see a clear trend that some detectors registered similar peak loads on repeated occasions while another registered significantly lower loads on repeated occasions. Besides the well-known large influence of the unknown impact position, this implies that besides the influence of the unknown impact position, the accuracy of the detectors to measure high-frequency dynamic loads needs to be verified. Further, based on the assessment of the ability of the detectors to measure mean load (carried out in figure 3.12), it can be concluded that the detectors seem not sufficiently calibrated. Variations in measured loads could also be due to variations in track stiffness and track geometry at different detector sites. Regardless of the reason it would be interesting to carry out a further assessment of the different detector types and detector sites for a better understanding of how good the detectors are to measure dynamic wheel-rail contact forces at high frequencies. Unfortunately, in the current study the procedure used for post-processing of measured data were unknown. This adds significant uncertainty to the comparison between detector data and simulation results.

The background to the project was to find out more about wheel-rail impact loads generated by wheel flats and to investigate whether the applied method of regulating maximum wheel flats size is reasonable. From the findings in this thesis, and if the measurement accuracy of the detectors can be verified, it seems more reasonable to base the regulations on measured peak loads. Since peak loads increase with increasing mean loads, this implies that a wheel flat on a wagon with a lower axle load is less detrimental compared to the same flat on a wagon with a higher axle load. Further, no clear correlation between flat length, train speed and peak load could be found. Thus, the method of basing the regulation on the measured length of the flat could not be supported in this thesis. Altogether, it seems reasonable to change the current regulation to allow unloaded wagons (low axle loads) continue operating until they reach their final destination with workshop capabilities as long as their registered peak loads from wheel impact load detectors do not exceed 280 kN. The reason why 350 kN is not suggested is to include a safety margin since the worst case of impact position might not occur while the wheel flat is within the detector. The safety margin was based on comparing the simulated results of the maximum peak load, presented in figure 5.9, to the mean of the peak loads presented in B.2, where it is possible to see that the value deviates around 70 kN for an axle load of 25 tonnes and speed 90 km/h. It is worth mentioning that even though the wheel flats analyzed in this work did not show peak loads exceeding 350 kN, wheels with wheel flats should be replaced as soon as possible to minimise deterioration and maximise safety of the tracks and vehicles. The overall aim of this thesis is to reduce unnecessary traffic disruptions while at the same time maintaining safety.

Regulations regarding the speed of a train with wheel flats could also be applied. In the literature review, it was presented that a local maximum in peak load has been observed for wheel flats at vehicle speeds of around 40 km/h. This is in agreement with Trafikverket's regulations where the speed interval 15-45 km/h should be avoided for a locomotive that triggers alarms in colder temperatures. A similar local maximum was observed in the simulations but at a higher speed for both of the studied wheel flats. The vehicle speed at the local maximum is dependent on the geometry of the flat, in particular the length of the tread damage. This makes it more complicated to specify a recommendation since a lower speed can make the situation worse for some flat lengths but not for others. To be able to present better recommendations, it would therefore be interesting to carry out a further investigation of how speed affects the magnitude of peak loads.

One of the objectives of the present work was to scan a wheel with a wheel flat that had been rolling on Stålpendeln, i.e. on the same route for which the analysis of detectors was carried out. The aim was to find a wheel that with certainty had passed several detectors after the wheel flat had been created, making it possible to compare simulations using the scanned wheel geometry as input with detector data. Unfortunately, this was not possible to arrange, and therefore old scanned wheels were used which had passed through detectors that were not included in the data analysis carried out in this report. For a further validation of WERAN, it would be

interesting to repeat this study to make an even better evaluation of how a given wheel flat geometry leads to different peak loads in different situations.

References

[1] A. Larsson and R.-M. Johansson, "Detektorer. Hantering av larm samt åtgärder efter konstaterade skador," 2022.

[2] A. Lundin, "Instruktion mätning av hjulplattor för lok och godsvagn," Unpublished, 2021, Technical report, Green Cargo.

[3] Trafikverket, "Hjulskador." available at https://trafikverket.ineko.se/Files/sv-SE/10393/RelatedFiles/100666_Hjulskador.pdf (2013).

[4] L. Fehrlund, Private communication, 2023.

[5] A. Alemi, F. Corman, Y. Pang, and G. Lodewijks, "Reconstruction of an informative railway wheel defect signal from wheel–rail contact signals measured by multiple wayside sensors," *Proceedings of the Institution of Mechanical Engineers, Part F: Journal of Rail and Rapid Transit*, vol. 233, no. 1, pp. 49–62, 2019.

[6] Trafikverket, "Detektorer i järnvägsanläggningen," available at https://bransch.trafikverket.se/for-dig-i-branschen/teknik/anlaggningsteknik/Detektorer/ (2023/01/23).

[7] R. Deuce, A. Ekberg, and E. Kabo, "Mechanical deterioration of wheels and rails under winter conditions – mechanisms and consequences," *Proceedings of the Institution of Mechanical Engineers, Part F: Journal of Rail and Rapid Transit*, vol. 13, no. 233.6, pp. 640–648, 2019.

[8] J. C. O. Nielsen, A. Pieringer, D. J. Thompson, and P. T. Torstensson, "Wheel–rail impact loads, noise and vibration: A review of excitation mechanisms, prediction methods and mitigation measures," *Noise and Vibration Mitigation for Rail Transportation Systems (Proceedings of the 13th International Workshop on Railway Noise (IWRN13), Ghent, Belgium, September 2019), Notes on Numerical Fluid Mechanics and Multidisciplinary Design*, vol. 150, p. 3–40, 2021.

[9] A. Lundin, Private communication, 24-05-2024.

[10] K. Larsson, "Wheel damage and maintenance of SCA Skog wagons," 2016.

[11] A. Pieringer, W. Kropp, and J. C. O. Nielsen, "The influence of contact modelling on simulated wheel/rail interaction due to wheel flats," *Wear*, vol. 314, no. 1, pp. 273–281, 2014.

[12] T. X. Wu and D. J. Thompson, "A hybrid model for the noise generation due to railway wheel flats," *Journal of Sound and Vibration*, vol. 251, pp. 115–139, 2002.

[13] A. Johansson and J. C. O. Nielsen, "Out-of-round railway wheels—wheel-rail contact forces and track response derived from field tests and numerical simula-

tions," *Proceedings of the Institution of Mechanical Engineers, Part F: Journal of Rail and Rapid Transit*, vol. 217, pp. 135 – 146, 2003.

[14] J. Jergéus, C. Odenmarck, R. Lundén, P. Sotkovszki, B. Karlsson, and P. Gullers, "Full-scale railway wheel flat experiments," *Proceedings of the Institution of Mechanical Engineers, Part F: Journal of Rail and Rapid Transit*, vol. 213.1, pp. 1–13, 1999.

[15] "Welcome to the GCU," https://gcubureau.org/, 13-06-2023.

[16] "Technical conditions for wagon transfers between railway undertakings, Appendix 9," *To the general contract of use (GCU) for wagons*, 2023-01-01.

[17] M. Asplund, "Larmnivåer hjulskadetektor TRV 2020/96962," Dec 2021.

[18] "Measuring eyes," https://www.schenckprocess.com/glossary/measuring-eyes, 2023.

[19] "PHOENIX MDS WDD/WIM wheel defect detection / Weighing in motion," https://www.voestalpine.com/railway-systems/en/products/phoenix-mds-wdd-wim-weighing-in-motion-wheel-defect-detection/.

[20] R. Byström, Private communication, 16-05-2023.

[21] D. Elfström, Private communication, 16-05-2023.

[22] Trafikverket, "Krav detektorer; förutbestämt underhåll detektoranläggningar i spårmiljö järnväg, TDOK 2019:0478," 2019.

[23] J. C. O. Nielsen, T. J. S. Abrahamsson, and A. Ekberg, "Probability of instant rail break induced by wheel–rail impact loading using field test data," *International Journal of Rail Transportation*, vol. 10, no. 1, pp. 1–23, 2022.

[24] N. T. V. Dang, "The effect of high wheel impact load on rail reliability – a case study at Bodsjön," Master's thesis, KTH Royal Institute of technnology, Stockholm, Sweden, 2021.

[25] J. Sandström and A. Ekberg, "Predicting crack growth and risks of rail breaks due to wheel flat impacts in heavy haul operations," *Proceedings of the Institution of Mechanical Engineers, Part F: J. Rail and Rapid Transit*, vol. 223, pp. 153–161, 2009.

[26] M. Asplund and P. Söderström, "Field validation of force response from defective wheel," *12th International Conference on Contact Mechanics and Wear of Rail/Wheel Systems (CM2022)*, September 2022.

[27] R. Hedström, "Genomförda utredningar och försök med längre och tyngre tåg i Sverige," Tech. Rep., 2013.

[28] "Matlab r2018b," Software, 2018. [Online]. Available: https://www.mathworks.com/products/matlab.html

[29] "Workshop employee at Euromaint," Private communication, 03-05-2023.

[30] "Green cargo ellok," Available at https://www.svenska-lok.se/motor.php?s=5&litra=Mb&typenr= (2023/04/05).

[31] L. Fehrlund, Private communication, 22-05-2023.

[32] M. Maglio, "Influence of railway wheel tread damage and track properties on wheelset durability – field tests and numerical simulations," Ph.D. dissertation, Chalmers University of Technology, Gothenburg, Sweden, 2023.

[33] "Handyscan, VX inspect and VX model." https://www.creaform3d.com/en, Creaform, Canada.

[34] E. Andersson and M. Berg, *Järnvägssystem och spårfordon. Del 2: Spårfordon*, ser. Järnvägsgruppen KTH. Stockholm: KTH högskoletryckeriet, 1999.

[35] "Kordasatsen," https://www.formelsamlingen.se/alla-amnen/matematik/geometri-i/kordasatsen, 2023.

[36] M. Maglio, A. Pieringer, J. C. O. Nielsen, and T. Vernersson, "Wheel–rail impact loads and axle bending stress simulated for generic distributions and shapes of discrete wheel tread damage," *Journal of Sound and Vibration*, vol. 502, 2021.

[37] A. Pieringer, "Time-domain modelling of high-frequency wheel/rail interaction," Ph.D. dissertation, Chalmers University of Technology, Gothenburg, Sweden, 2011.

[38] M. Maglio, T. Vernersson, J. C. O. Nielsen, A. Ekberg, and E. Kabo, "Influence of railway wheel tread damage on wheel–rail impact loads and the durability of wheelsets," *Submitted for international publication*, 2023.

[39] A. Pieringer and W. Kropp, "A fast time-domain model for wheel/rail interaction demonstrated for the case of impact forces caused by wheel flats," *Proceedings of Acoustics'08,Paris, France*, June 29-July 4, 2008.

A

Appendix A - Additional results from analysis of detector data

A.1 Dynamic load - Influence of train speed for different flat length intervals

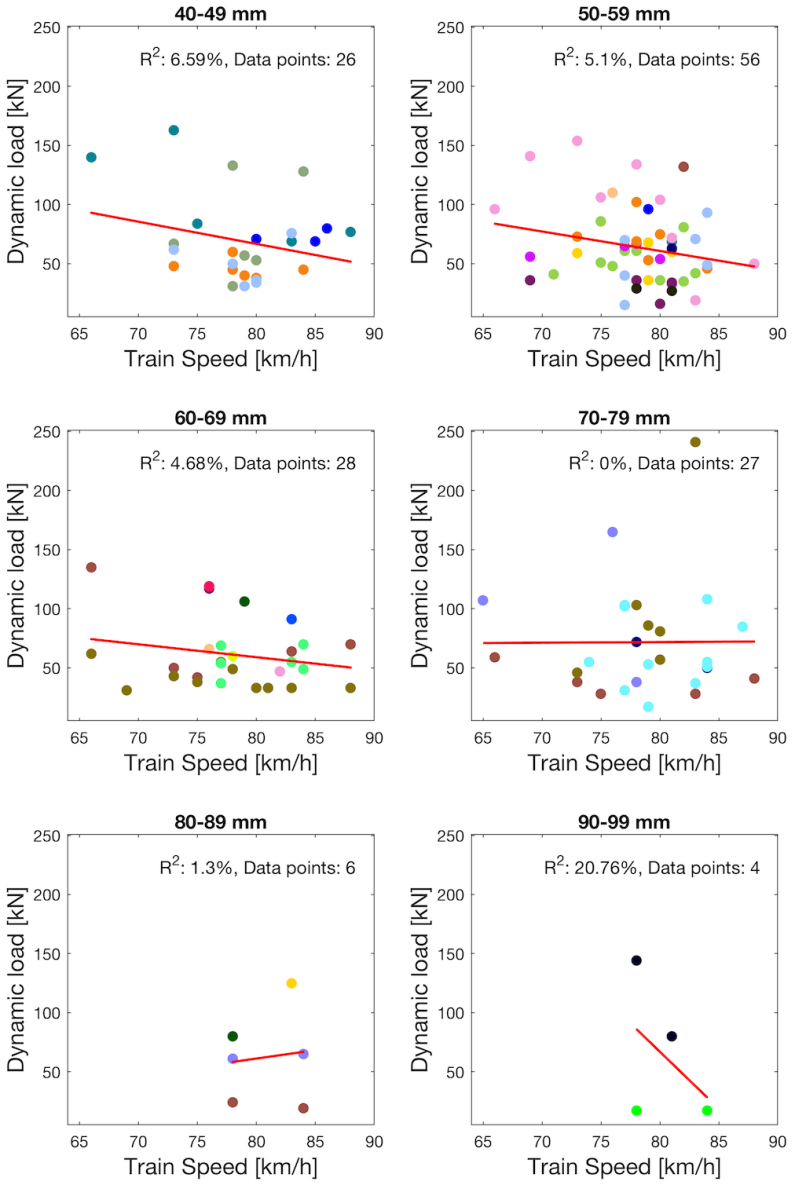

Figure A.1: Influence of flat length and train speed on measured dynamic load. Loaded wagons weighing between 17-25 tonnes.

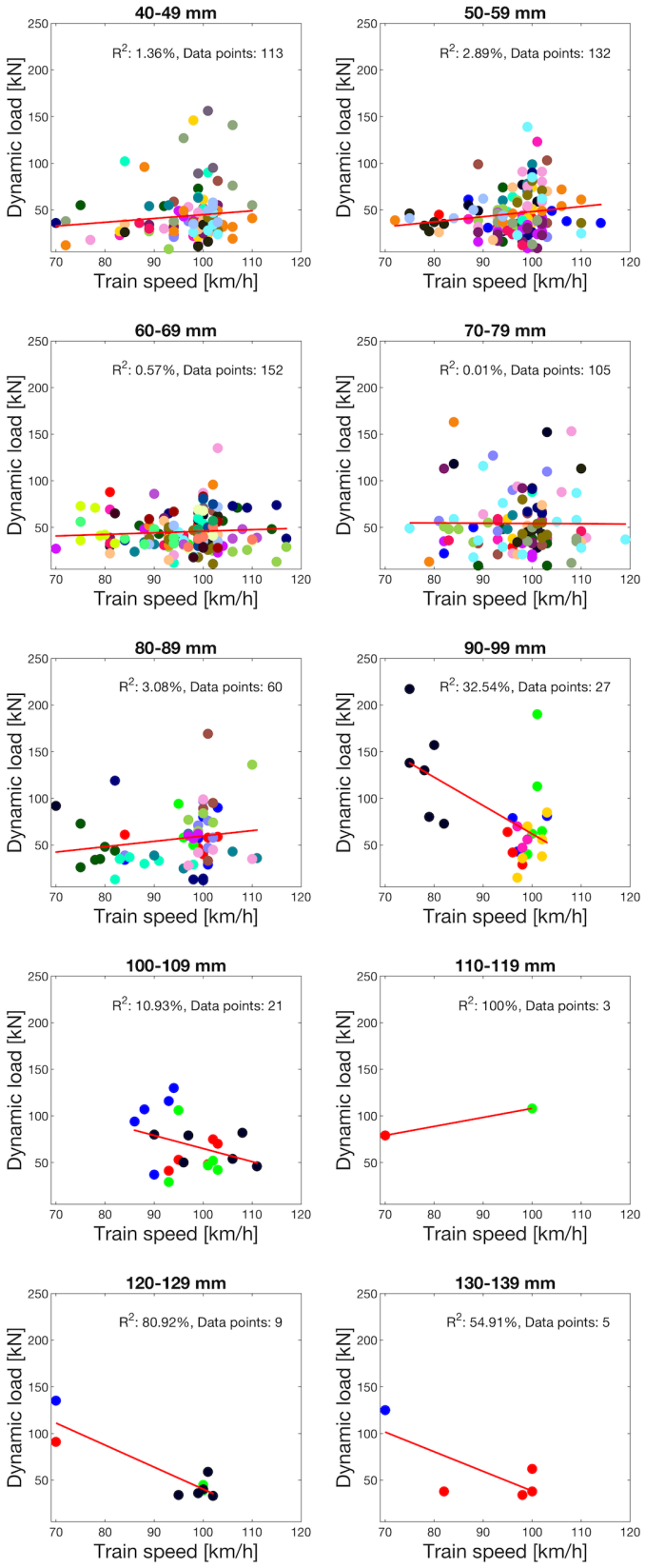

Figure A.2: Influence of flat length and train speed on measured dynamic load. Unloaded wagons weighing between 4.5-6 tonnes.

A.2 Ratio - Influence of train speed for different flat length intervals

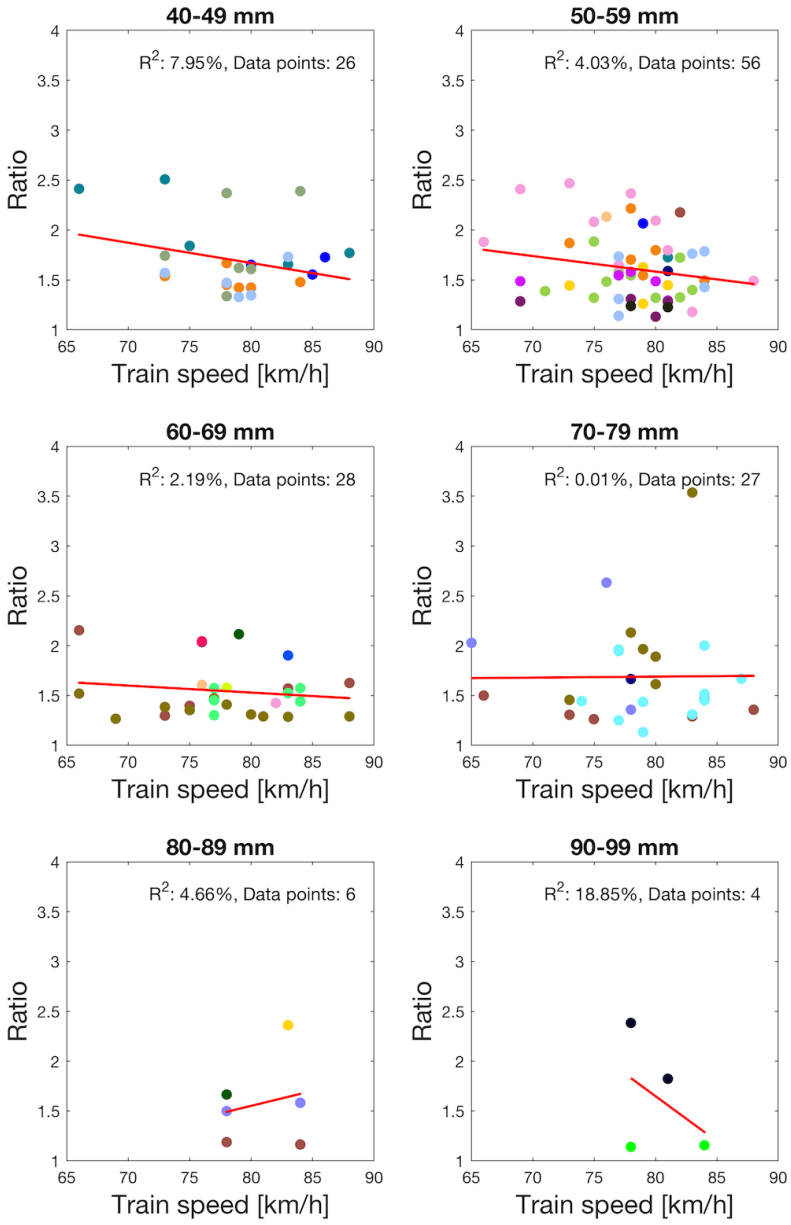

Figure A.3: Influence of flat length and train speed on measured ratio. Loaded wagons weighing between 17-25 tonnes.

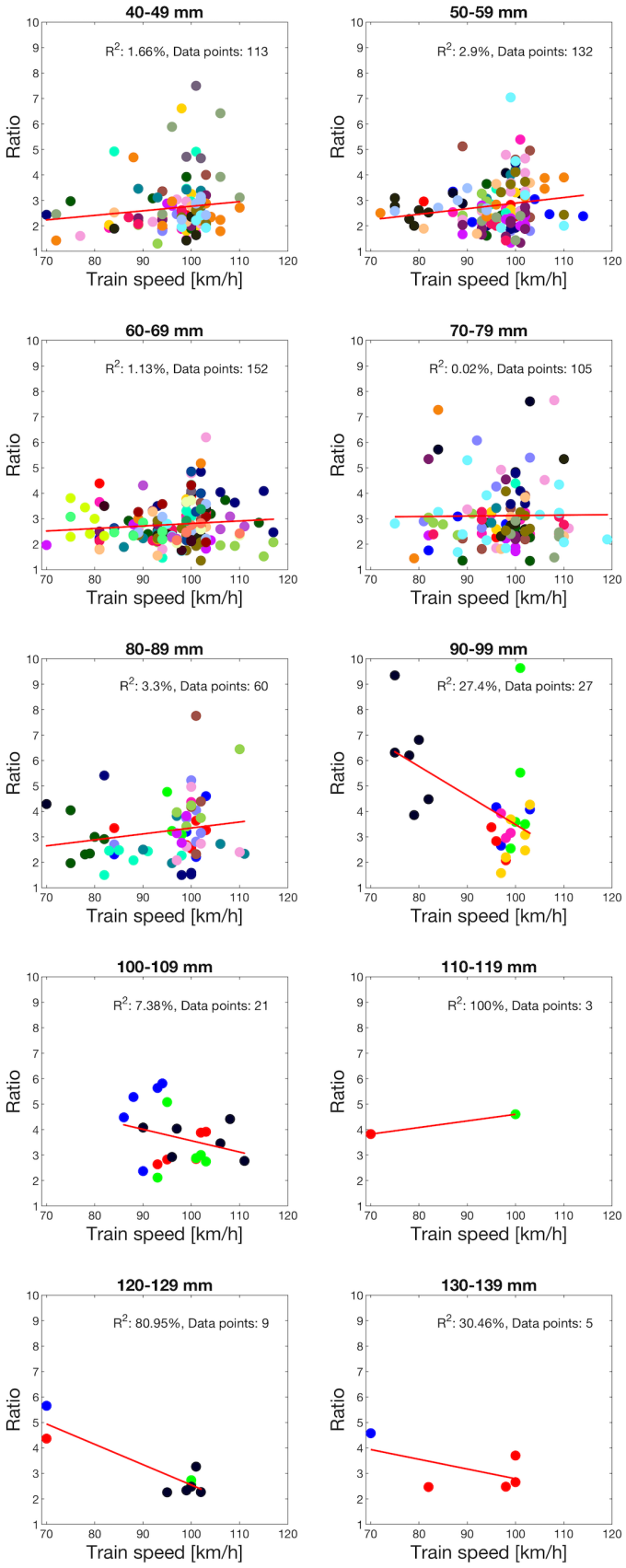

Figure A.4: Influence of flat length and train speed on measured ratio. Unloaded wagons weighing between 4.5-6 tonnes.

A.3 Peak loads - Influence of flat length in different train speed intervals

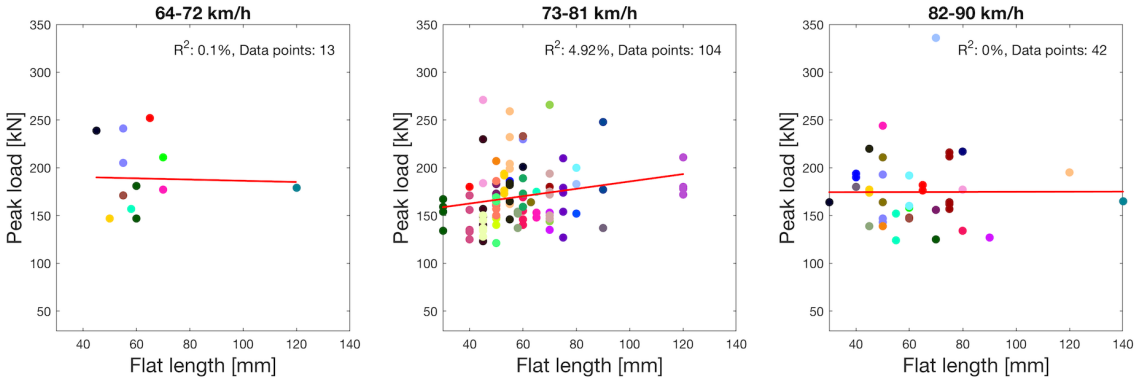

Figure A.5: Influence of flat length and train speed on measured peak loads. Loaded wagons weighing between 17-25 tonnes.

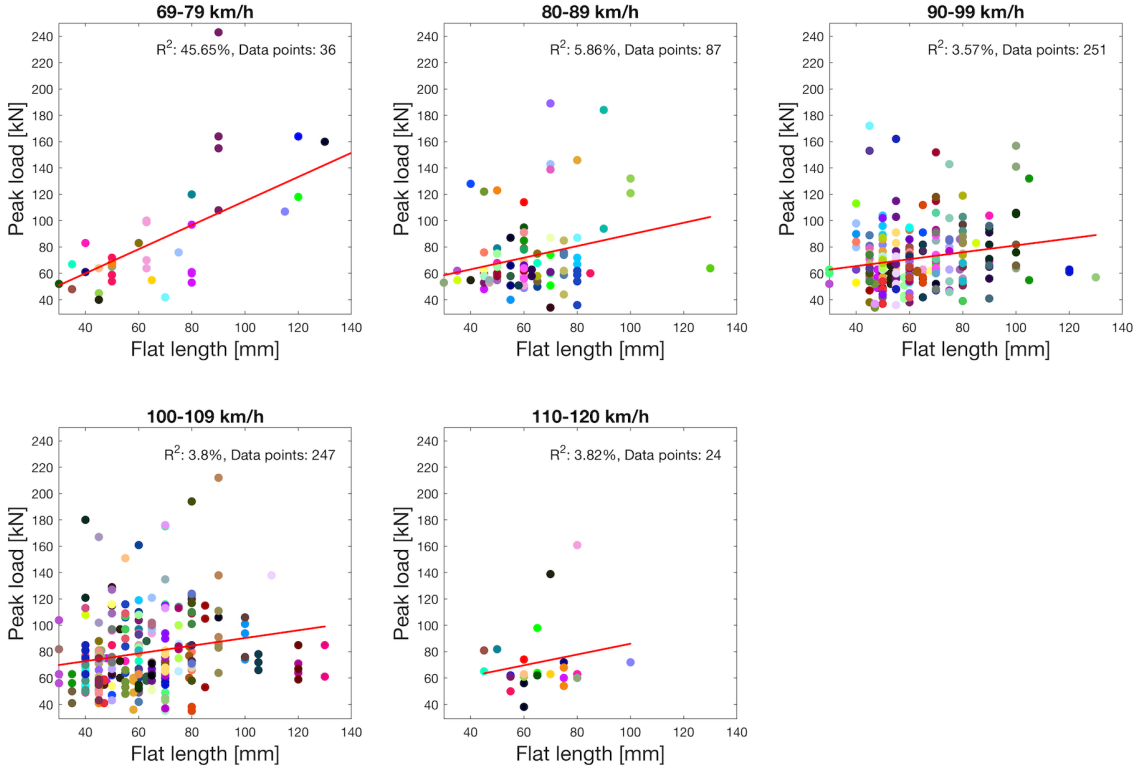

Figure A.6: Influence of flat length and train speed on measured peak loads. Unloaded wagons weighing between 4.5-6 tonnes.

B

Appendix B - Additional results from simulations

B.1 Mean load and standard deviation

To get an understanding of how the position of where the flat hits the rail within the sleeper bay influences the scatter in magnitudes of the wheel-rail impact load, the mean and standard deviation of the simulated peak loads are presented. For each combination of train speed and axle load, the presented values are based on the 16 different peaks loads from the simulations (eight in each direction). The plots presented are from the simulations with the non-reprofiled wheels.

B.1.1 Wheel flat 1

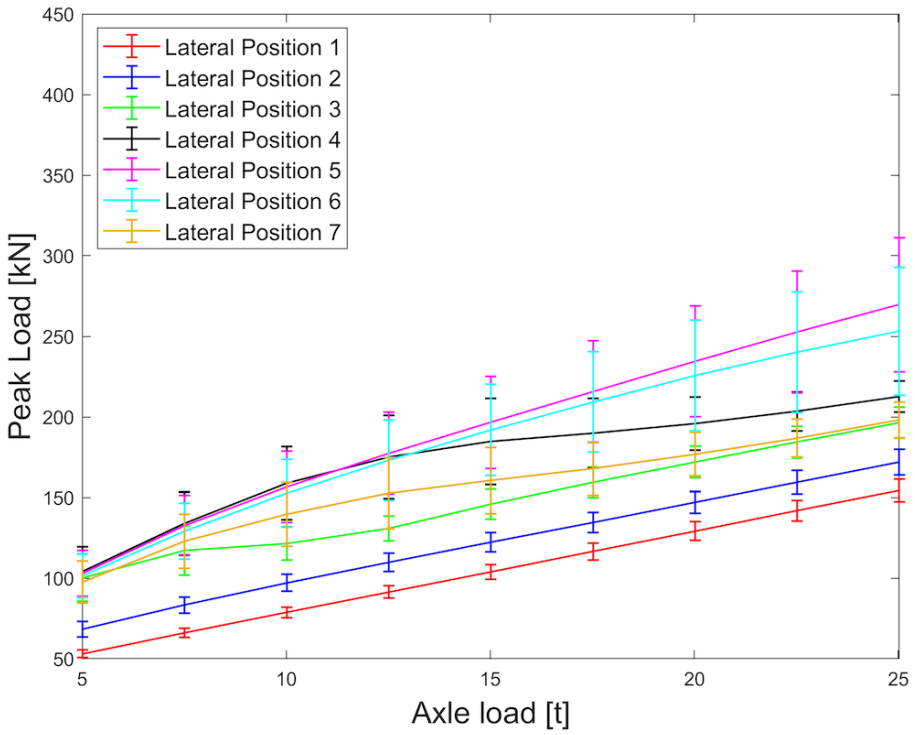

Figure B.1: Influence of axle load on mean and standard deviation of simulated peak load. Wheel flat 1 and train speed 100 km/h

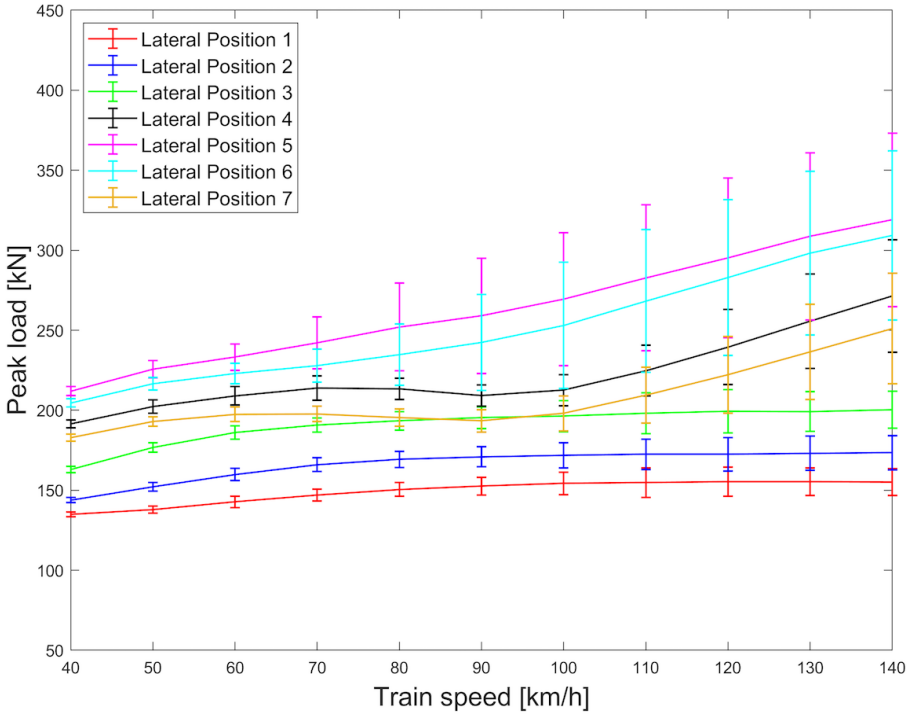

Figure B.2: Influence of train speed on mean and standard deviation of simulated peak load. Wheel flat 1 and axle load 25 tonnes

B.1.2 Wheel flat 2

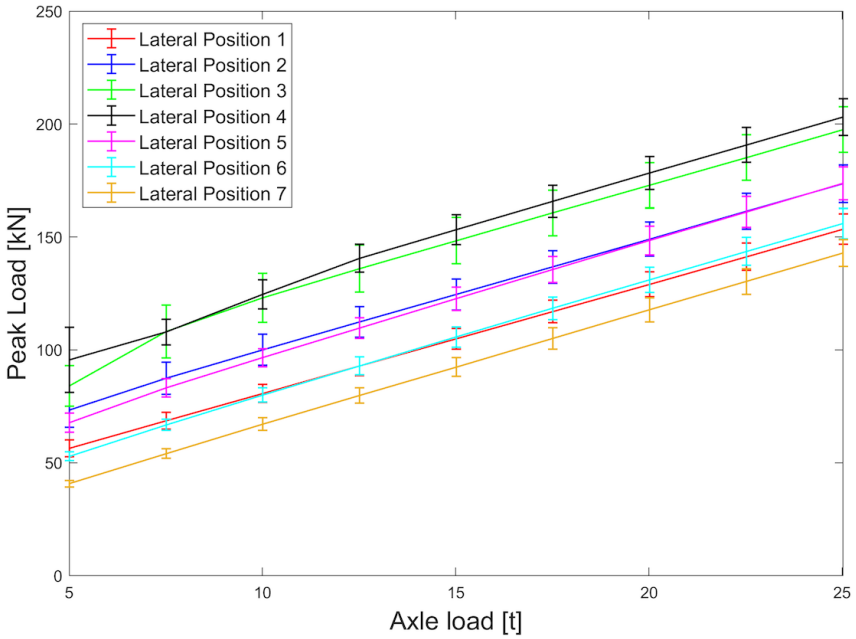

Figure B.3: Influence of train speed on mean and standard deviation of simulated peak load. Wheel flat 2 and train speed 100 km/h.

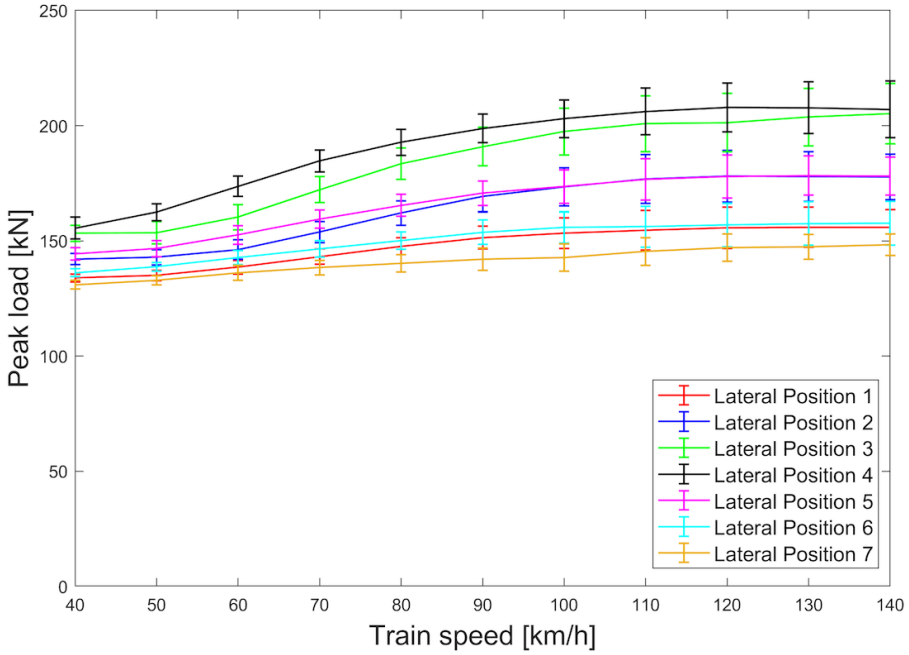

Figure B.4: Influence of axle load on mean and standard deviation of simulated peak load. Wheel flat 2 and axle load 25 tonnes.

B.2 Maximum dynamic loads

The dynamic loads are presented for the lateral position which gave rise to the highest forces during the simulations. Figures B.5 and B.6 can be compared with the corresponding peak loads presented in figures 5.12 and 5.15

B.2.1 Wheel flat 1

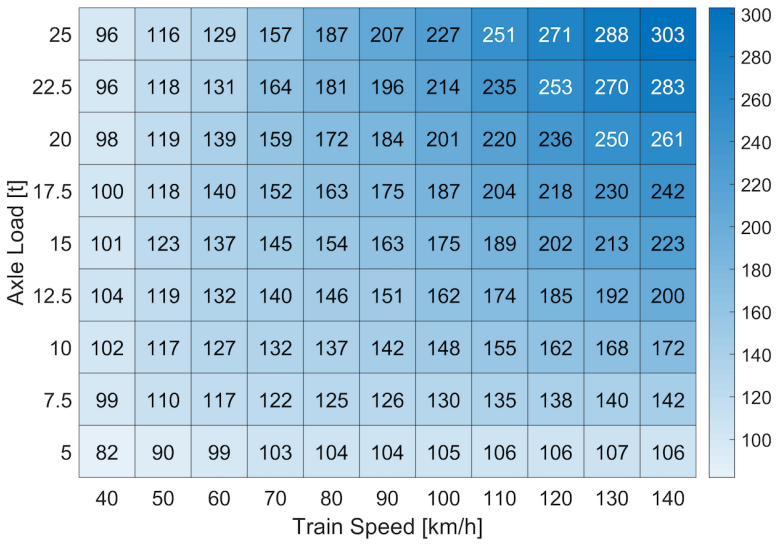

Figure B.5: Wheel flat 1: Influence of train speed and axle load on maximum dynamic load in [kN]. Lateral contact position 6

B.2.2 Wheel flat 2

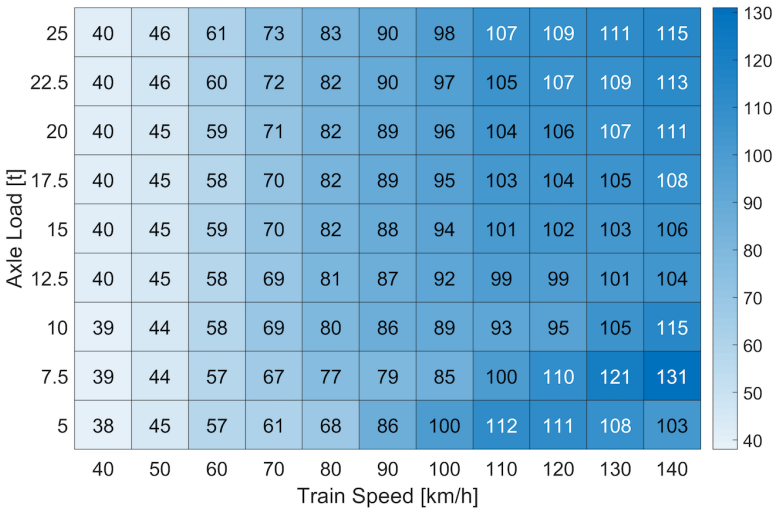

Figure B.6: Wheel flat 2: Influence of train speed and axle load on maximum dynamic load in [kN]. Lateral contact position 7

DEPARTMENT OF SOME SUBJECT OR TECHNOLOGY
CHALMERS UNIVERSITY OF TECHNOLOGY
Gothenburg, Sweden
www.chalmers.se

CHALMERS
UNIVERSITY OF TECHNOLOGY